

A Versatile Sub-Nanomolar Fluorescent Ligand Enables NanoBRET Binding Studies and Single-Molecule Microscopy at the Histamine H₃ Receptor

Niklas Rosier, Lukas Grätz,* Hannes Schihada, Jan Möller, Ali Işbilir, Laura J. Humphrys, Martin Nagl, Ulla Seibel, Martin J. Lohse, and Steffen Pockes*



Cite This: <https://doi.org/10.1021/acs.jmedchem.1c01089>



Read Online

ACCESS |



Metrics & More

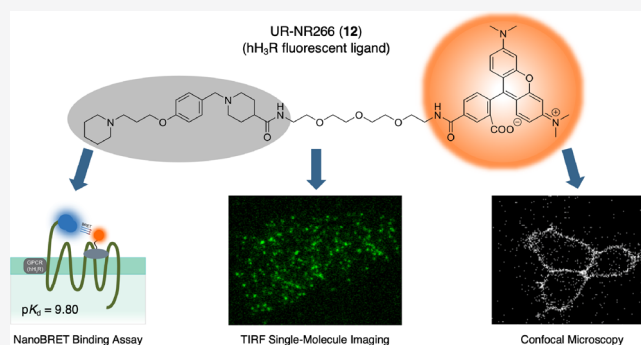


Article Recommendations



Supporting Information

ABSTRACT: The histamine H₃ receptor (H₃R) is considered an attractive drug target for various neurological diseases. We here report the synthesis of UR-NR266, a novel fluorescent H₃R ligand. Broad pharmacological characterization revealed UR-NR266 as a sub-nanomolar compound at the H₃R with an exceptional selectivity profile within the histamine receptor family. The presented neutral antagonist showed fast association to its target and complete dissociation in kinetic binding studies. Detailed characterization of standard H₃R ligands in NanoBRET competition binding using UR-NR266 highlights its value as a versatile pharmacological tool to analyze future H₃R ligands. The low nonspecific binding observed in all experiments could also be verified in TIRF and confocal microscopy. This fluorescent probe allows the highly specific analysis of native H₃R in various assays ranging from optical high throughput technologies to biophysical analyses and single-molecule studies in its natural environment. An off-target screening at 14 receptors revealed UR-NR266 as a selective compound.



INTRODUCTION

The histamine H₃ receptor (H₃R) is a seven-transmembrane domain receptor and belongs to the superfamily of G-protein coupled receptors (GPCRs).¹ The H₃R represents one of four members of the histamine receptor family and mediates its G-protein-dependent signaling mainly via G_i-proteins.^{2,3} Due to the fact that the H₃R is almost exclusively expressed in the brain,^{1,4–6} it is an interesting target for numerous diseases of the central nervous system, such as Parkinson's,⁷ Huntington's,^{8,9} and Alzheimer's diseases,¹⁰ as well as tic disorders.¹¹ In 2016, the inverse agonist pitolisant entered the market as the first (and until now only) drug targeting the H₃R for the treatment of narcolepsy.¹² In addition, pitolisant has shown promising results in initial studies for the treatment of Prader–Willi Syndrome.¹³ Accordingly, the H₃R is a highly interesting target for CNS-related diseases and urgently needs to be studied in more detail at the molecular level.

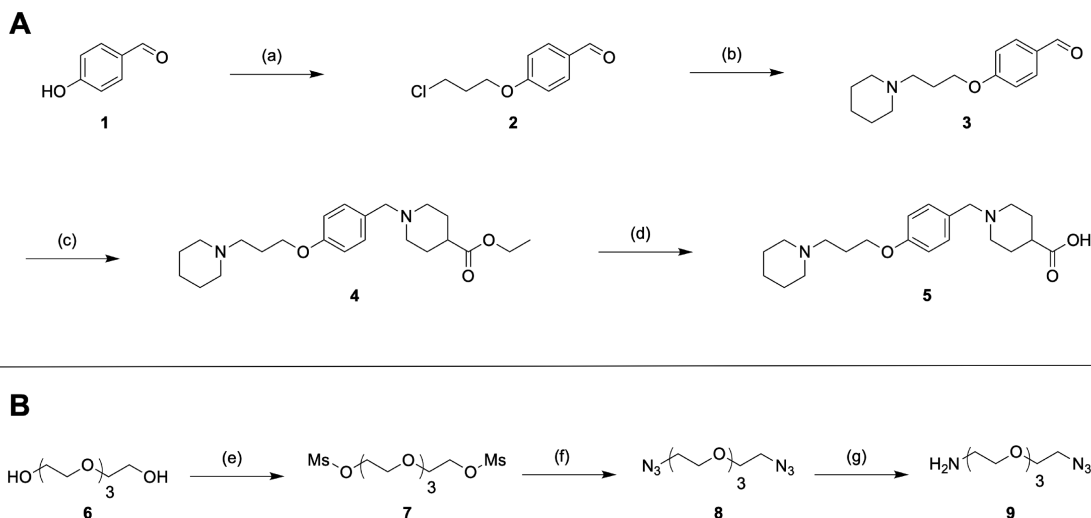
Fluorescently labeled ligands and related methods have gained increasing importance in modern GPCR research. The methods to be mentioned here include resonance energy transfer (RET) assays, fluorescence anisotropy, and fluorescence correlation spectroscopy. Over the last decade, time-resolved Förster/bioluminescence resonance energy transfer (TR-FRET/BRET) techniques have become increasingly important in the study of ligand binding at GPCRs to provide

information on ligand–receptor interactions.^{14–16} Among many imaging technologies, total internal reflection fluorescence (TIRF) microscopy represents the most advanced method for single-molecule imaging of individual proteins within (or close to) the plasma membrane.^{17,18} Although several fluorescent H₃R ligands have already been reported,^{19–22} none of them has been shown to be suitable for single-molecule studies. We therefore aimed to develop a tool suitable for single-molecule imaging and as a tracer probe for binding studies of new putative drug candidates for the H₃R in a recently developed NanoBRET binding assay that can be employed in high throughput analyses.²³

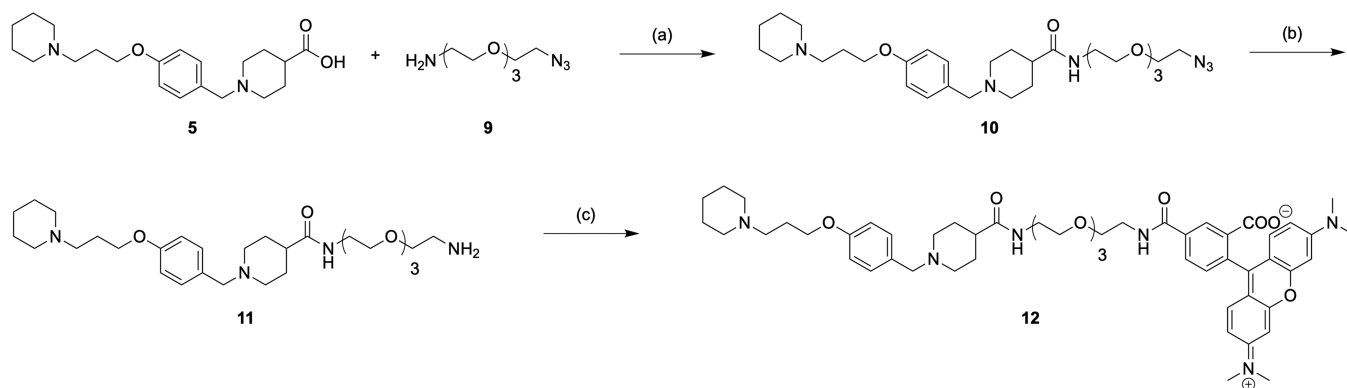
RESULTS AND DISCUSSION

Design Rationale. Fluorescent receptor ligands can be considered as a combination of three distinct parts: the parent ligand, often referred to as a pharmacophore, a linker region,

Received: June 17, 2021

Scheme 1. Synthesis of the Pharmacophoric H₃R Scaffold 5 (A) and the Linking PEG Structure 9 (B)^a

^aReagents and conditions: (a) 1-Br-3-Cl-propane, K₂CO₃, MeCN, reflux, 18 h, 89%; (b) piperidine, Na₂CO₃, KI, MeCN, reflux, 20 h, 76%; (c) ethyl isonipicotate, NaBH(OAc)₃, CHCl₃, rt, overnight, 95%; (d) 2 N HCl, THF, rt, overnight, 92%; (e) methane sulfonyl chloride, NEt₃, DCM, rt, overnight, 78%; (f) NaN₃, EtOH/DMF (4:1), reflux, overnight, 90%; (g) PPh₃, 1 N HCl/THF/EtOAc (5:1:5), rt, overnight, 77%.

Scheme 2. Synthesis of the 5-TAMRA-Labeled Fluorescent H₃R Ligand 12^a

^aReagents and conditions: (a) 1. 5, EDC·HCl, HOBT, DIPEA, DCM/DMF (1:1), rt, 30 min; 2. 9, 100 °C, MW, 30 min, 65%; (b) 1. 10, PPh₃, THF, 4 h, 45 °C; 2. H₂O, 2 h, 45 °C, 60%; (c) 1. 11, 5-TAMRA NHS ester, NEt₃, DMF, rt, 2.5 h; 2. 10% aq. TFA, rt, 15 min, 82%.

and a fluorescent dye. Each of them has to be chosen depending on the intended use of the final fluorescent ligand.²⁴

The H₃ receptor antagonist JNJ-5207852, one of the most affine H₃ receptor ligands reported so far, has been used as the parent ligand. Besides its high H₃R affinity, it shows an excellent selectivity not only within the histamine receptor family but also with respect to 50 other different targets.²⁵ These properties combined with synthetic accessibility and good water solubility make it an excellent pharmacophore for a fluorescent ligand. Structure activity relationships showed a high tolerance of the ligand toward structural changes at the para position of the benzylic piperidine moiety.²⁶ Thus, this position of the molecule has been chosen to attach the linker via an amide group.

In terms of the linker moiety, a flexible polyethyleneglycol-based (PEG-based) structure with a length of 13 atoms was used, which we assumed would be sufficient to reach outside the binding pocket, thus reducing the probability of a negative impact of the linker on ligand binding. PEG-based linkers are often used in fluorescent ligands, as they are chemically stable,

show higher water solubility than alkylic structures, and are less susceptible to interact with cell membranes.²⁷

The choice of the fluorescent dye must be taken carefully for any fluorescent ligand and depends mainly on the intended application of the ligand. With the aim of a versatile fluorescent ligand for use in the NanoBRET binding assay and fluorescence microscopy, the 5-TAMRA fluorescent dye was chosen. The suitability of this dye for NanoBRET binding has been shown for different receptors,^{15,16} as it led to a better signal to noise ratio and less adhesion to the plastic vessel than, e.g., BODIPY labeled ligands at the H₂ receptor.²⁸ Furthermore, 5-TAMRA was reported as a fluorescent dye for single molecule imaging in TIRF microscopy,^{29,30} and due to its hydrophilicity, it is less prone to interact with cell membranes than BODIPY,³¹ resulting in a lower nonspecific binding in fluorescence microscopy techniques.

Chemistry. The synthesis of the fluorescent ligand's pharmacophore 5 was carried out, following publications by Apodaca et al. and Wingen et al. with minor modifications, obtaining excellent yields (Scheme 1A).^{25,26} Starting from 4-hydroxybenzaldehyde (1), 2 was obtained in a nucleophilic

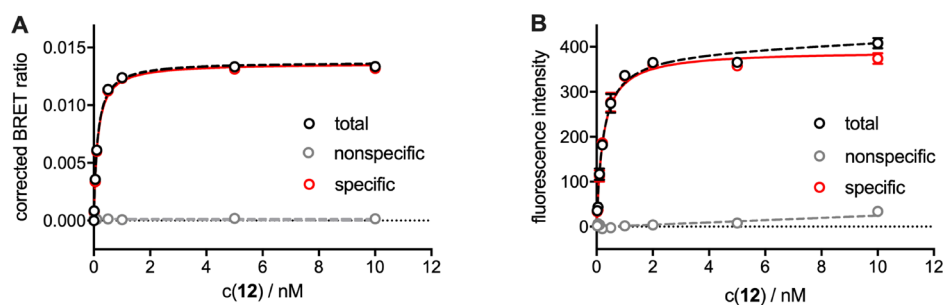


Figure 1. Representative isotherms from saturation binding experiments with **12** at the NLuc-hH₃R (A, NanoBRET) and at the wild-type hH₃R (B, flow cytometry), both stably expressed in HEK293 cells.

Table 1. Comparison of Thermodynamic and Kinetic Binding Constants of **12 at the Wild-Type hH₃R and the NLuc-hH₃R**

compound	flow cytometry				NanoBRET binding			
	pK_d (sat) ^a	pK_d (sat) ^b	k_{obs} ^c (min ⁻¹)	τ_{ass} ^d (min)	k_{off} ^e (min ⁻¹)	τ_{diss} ^e (min)	k_{on} ^f (min ⁻¹ nM ⁻¹)	pK_d (kin) ^g
12	9.71 ± 0.04	9.80 ± 0.07	0.51 ± 0.02	1.97 ± 0.14	0.16 ± 0.01	6.45 ± 0.62	0.71 ± 0.04	9.66 ± 0.15

^aData represent mean values ± SEM from three independent experiments each performed in duplicate. Flow cytometric measurements performed with HEK293-SP-FLAG-hH₃R (wild-type hH₃R) cells. ^bData represent mean values ± SEM from three independent experiments each performed in triplicate. NanoBRET binding experiments performed with live HEK293 cells stably expressing the NLuc-hH₃R. ^cData represent mean values ± SEM from four independent experiments. ^dAssociation time constant: $\tau_{ass} = 1/k_{obs}$. Data represent mean values ± CI (95%) from four independent experiments. ^eDissociation time constant: $\tau_{diss} = 1/k_{off}$. Data represent mean values ± CI (95%) from four independent experiments. ^fAssociation rate constant: $k_{on} = (k_{obs} - k_{off})/c(12)$. Indicated errors were calculated according to the Gaussian law of error propagation. ^g K_d (kin) = k_{off}/k_{on} ; pK_d (kin) = $-\log K_d$ (kin). Indicated errors were calculated according to the Gaussian law of error propagation.

substitution reaction with 1-bromo-3-chloropropane. The same reaction type using piperidine resulted in aldehyde **3**. A reductive amination with ethyl isonipecotate, using sodium triacetoxyborohydride as a reductive agent in chloroform, yielded **4**. Acid catalyzed hydrolysis of **4** afforded the free acid **5** as a dihydrochloride.²⁶

The synthesis of the linker (Scheme 1B), which is necessary for the connection of the pharmacophore with the fluorophore, started from the commercially available tetraethylene glycol **6**. In the first step, mesylate groups were introduced (**7**) as good leaving groups, followed by subsequent treatment with sodium azide to afford **8**.^{32,33} A selective “Staudinger”-type reduction of a single azide group in a biphasic water/ethyl acetate mixture afforded the final linker **9** with 77% yield.³⁴

Subsequently, **5** was coupled with **9** using EDC/HOBt as coupling reagents under microwave irradiation to afford product **10**,²⁶ which was reduced to the primary amine **11** by a “Staudinger” reaction (Scheme 2). In the final step, **11** was coupled with the 5-TAMRA NHS ester in DMF to afford fluorescent ligand UR-NR266 (**12**, Scheme 2).²⁸ After preparative HPLC purification, **12** was obtained with high purity (99%) and yield (82%). The fluorescent ligand was further examined for its chemical stability in aqueous solution and showed no decomposition within an incubation period of 6 months (cf. Figure S1, Supporting Information (SI)). Fluorescence properties of **12** (in PBS containing 1% bovine serum albumin (BSA)) were ascertained by recording its excitation and emission spectra shown in Figure S2 (SI) and measuring the quantum yield ($\Phi = 35.09\%$ (in PBS), $\Phi = 33.31\%$ (in PBS + 1% BSA); cf. Table S1 in the SI). The 5-TAMRA-labeled ligand exhibited an excitation maximum at 555 nm and an emission maximum at 585 nm.

Pharmacological Characterization. The first step in the pharmacological characterization of the fluorescent ligand **12**, structurally derived from the H₃R antagonist JNJ-5207852 (JNJ)²⁵ (Figure S4, SI), was the investigation of the binding behavior in different assays. To achieve one of our main goals,

the compound was tested for suitability in the NanoBRET binding assay at the NLuc-hH₃R stably expressed in HEK293 cells. BRET saturation experiments provided a binding constant for **12** in the sub-nanomolar range ($pK_d = 9.80 \pm 0.07$, cf. Figure 1A; Table 1) and very low nonspecific binding. In order to investigate a potential influence of the receptor modification on ligand binding, **12** was additionally examined in flow cytometry using wild-type hH₃R cells (HEK293-SP-FLAG-hH₃R) (cf. Figure 1B).

The receptor affinity of **12** to wild-type H₃R ($pK_d = 9.71 \pm 0.04$, Table 1) was in the same range as for the NLuc-hH₃Rs showing no significant difference ($p < 0.05$, two-tailed *t*-test). This experimental setup further confirmed the minimal nonspecific binding of this ligand observed in the BRET assay. To further characterize the fluorescent tracer, radioligand competition binding experiments were performed at the H₁₋₄R, providing information on receptor subtype selectivity within the histamine receptor family. The ligand exhibited receptor affinity to the H₃R in a sub-nanomolar range with a pK_i of 9.52 ± 0.08 and an outstanding selectivity profile being at least 100,000-fold selective toward the human H₁R, H₂R and H₄R (cf. Figure 2; Table 2). Precursor compounds **4**, **5**, and **11** and reference compound JNJ-5207852 (JNJ) displayed H₃R affinities in the same range (Table 2). While pK_i data of **4** are in very good agreement with literature data (9.56 vs 9.64²⁶), we saw a difference for compound **5** (8.80 vs 7.89²⁶).

Being aware of the fact that the fluorescent ligand's pharmacological mode of action is crucial, e.g., since an agonist might distort apparent affinities of competitive ligands due to internalization processes and induction of ternary complex formation (ligand/H₃R/G-protein), we wanted to gain insights into the functional behavior of **12**. Therefore, we employed a recently developed BRET-based G₁₂ biosensor detecting G protein activation as a decrease in BRET between NLuc-tagged G_{α12} and cpVenus-tagged G_{γ2}.³⁷ We first determined the potency of the selective H₃R agonist imetit using the G₁₂ biosensor and HEK293A cells overexpressing the

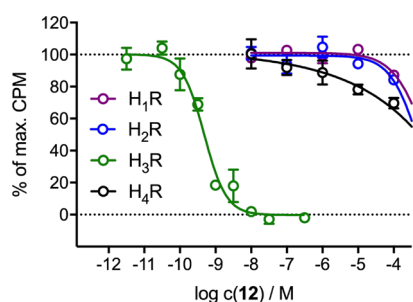


Figure 2. Displacement curves from radioligand competition binding experiments performed with compound **12** and the respective radioligands (cf. Table 2 footnotes).

wild-type H₃R (Figure S3, SI).³⁷ As expected, **12** acted as a neutral antagonist (Figure 3A) revealing a pK_b value of 9.04 ± 0.03 in competition experiments with the selective H₃R agonist imetit (Figure 3B). However, before using **12** as a molecular tool to characterize other H₃R ligands, the kinetic behavior of the fluorescent ligand should be determined first. The NanoBRET setup is ideally suited for this purpose due to the possibility to perform real-time kinetic measurements. 500 pM **12** was used to measure ligand association at the H₃R (Figure 4). Ligand binding to the receptor saturated after about 15 min ($\tau_{\text{ass}} = 1.97 \pm 0.14$ min), and the ligand fully dissociated with a tau (τ) value of 6.45 ± 0.62 min upon addition of an excess of clobenpropit (500-fold, $c = 250$ nM, Figure 4; Table 1). All kinetic parameters describing the binding of **12** in the BRET binding assay are presented in Table 1.

The complete reversibility of receptor binding makes the fluorescent ligand a suitable tool for use in competition binding studies, in our case, performed with a selection of standard H₃R agonists and antagonists (see structures in Figure S4, SI). We selected histamine (his),³⁸ imetit (imet),³⁹ (R)-(-)- α -methylhistamine (RAMH),⁴⁰ and (S)-(+)- α -methylhistamine (SAMH)⁴⁰ as agonists and clobenpropit (clob),⁴¹ Z27743747 (Z-cmpd),⁴² thioperamide (thio),⁴⁰ pitolisant (pito),⁴³ and JNJ-5207852 (JNJ)²⁵ as the inverse agonists/antagonists. For all ligands, total displacement could be determined with Hill slopes around 1 (Figure 5). Overall, our data are in good agreement with data from the literature (cf. Table 3), apart from RAMH and SAMH showing larger deviations. However, it is remarkable that the assay can distinguish between the two

enantiomers RAMH and SAMH, a phenomenon that has been described several times at the hH₃R (Table 3).^{40,44–46}

Fluorescence Microscopy. To visualize the binding and dissociation kinetics of the fluorescent ligand, we used confocal microscopy imaging. In this experiment, time-lapse images of HEK293-SP-FLAG-hH₃R cells were acquired (Figure 6). Compared to the kinetic NanoBRET experiments, we used 10 times higher concentrations of **12** to facilitate visualization with a confocal microscope. After the addition of **12** ($c = 5$ nM), the fluorescence signal on the cell surface increased and reached a plateau within 4 min (Figure 7A). The fluorescent ligand's dissociation was initiated by the addition of 2.5 μ M clobenpropit (500-fold excess). The addition of clobenpropit (after 220 s) decreased the fluorescence signal, indicating the dissociation of **12** (Figure 7B). We observed a τ value of 0.48 ± 0.07 min for the association and 3.50 ± 0.46 min for the dissociation of the fluorescent ligand (Table 4). These experiments demonstrated again that the binding of the fluorescent ligand to the H₃R occurs very rapidly and that the bound ligand can be displaced completely, similar to the results observed in the BRET binding assay. Due to the use of different concentrations (see above), a difference in k_{obs} values was to be expected (cf. Tables 1 and 4). However, the k_{on} and k_{off} values, which would be expected to be the same, differ by a factor of nearly 2 (cf. Tables 1 and 4). This could be a result of the receptor's modification with the NanoLuc, which may influence the binding kinetics. Consequently, the kinetic pK_d values from the NanoBRET (pK_d = 9.66 ± 0.15) and confocal experiments (pK_d = 9.10 ± 0.06) differ but are still in good agreement, so both assays can be considered complementary (cf. Tables 1 and 4). Additionally, we tested the photobleaching properties of **12** by immobilizing the fluorescent ligand in a 0.5% agarose film in 1 μ M final concentration. In these experiments, the ligand shows negligible photobleaching (4%, $N = 4$) after 20 min, which is unlikely to affect the observed association and dissociation kinetics of **12**. The biphasic curve describing the photobleaching properties is shown in Figure S28 in the SI.

Due to the low nonspecific binding and the high affinity of our compound, we wondered about its suitability for total internal reflection fluorescence (TIRF) single-molecule microscopy as shown previously for a few other fluorescent GPCR ligands.^{49–51} Indeed, its favorable properties were confirmed in microscopy experiments and allowed the acquisition of single-molecule TIRF movies in the presence

Table 2. Binding and Functional Data of **12** on Human Histamine Receptor Subtypes

compound	radioligand competition binding ^a								H ₃ R selectivity		G ₁₂ activation ^b	
	pK _i				K _i (H _{1,2,4} R)/K _i (H ₃ R)				pK _b			
	hH ₁ R ^c	N	hH ₂ R ^d	N	hH ₃ R ^e	N	hH ₄ R ^f	N	hH _{1,2,4} R	hH ₃ R ^g	N	
12	<4	3	<4	3	9.52 ± 0.08	3	<4	3	>100,000	9.04 ± 0.03	3	
4	n.d.		n.d.		9.56 ± 0.12	3	n.d.			n.d.		
5	n.d.		n.d.		8.80 ± 0.11	3	n.d.			n.d.		
11	n.d.		n.d.		9.40 ± 0.10	3	n.d.			n.d.		
JNJ	n.d.		n.d.		9.68 ± 0.01	3	n.d.			n.d.		

^aCompetition binding assay at HEK293-SP-FLAG-hH₁R, HEK293-SP-FLAG-hH₂R, HEK293-SP-FLAG-hH₃R, or HEK293-SP-FLAG-hH₄R cells.

^bCompetition binding experiment at HEK293A cells stably expressing the G₁₂ BRET sensor with the wild-type hH₃R. ^cDisplacement of 5 nM [³H]mepyramine (K_d = 4.5 nM). ^dDisplacement of 20 nM [³H]UR-DE257³⁵ (K_d = 66.9 nM). ^eDisplacement of 2 nM [³H]UR-PI294³⁶ (K_d = 5 nM). ^fDisplacement of 15 nM [³H]histamine (K_d = 15.88 nM). ^gInhibition of imetit-induced ($c = 1$ nM, EC₅₀ = 0.85 nM) G₁₂ activation. Data shown are mean values ± SEM of N independent experiments, each performed in triplicate. Data were analyzed by nonlinear regression and were best fitted to sigmoidal concentration–response curves. Displacement curves are presented in Figures 2 and 3.

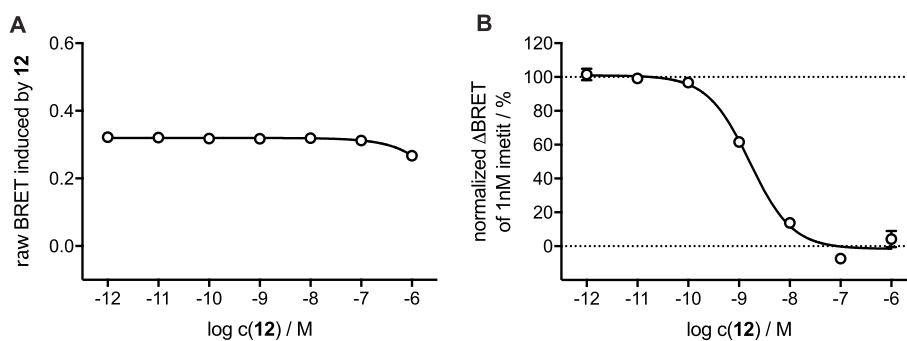


Figure 3. Concentration–response curves (CRCs) for G_i activation of **12** in the absence (A) and presence (B) of 1 nM imetit at HEK293A cells transiently expressing the G_{i2} BRET sensor along with the wild-type hH_3R .

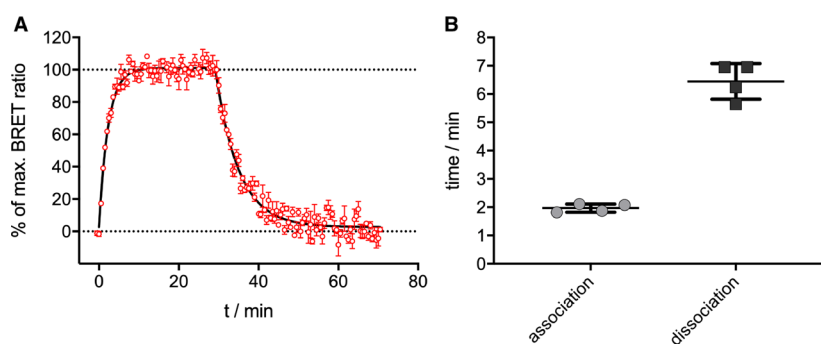


Figure 4. BRET-based specific binding kinetics of the fluorescent ligand **12** at the NLuc- hH_3R , stably expressed in HEK293 cells. (A) Graph shows association of **12** ($c = 500$ pM) to the receptor and dissociation of **12** induced by addition of clobenpropit ($c = 250$ nM, 500-fold excess) from a representative experiment. (B) Scatter dot plot displaying the quantification of tau (τ) values for association/dissociation of the fluorescent ligand. Data were analyzed from four independent experiments and are represented as mean \pm SD.

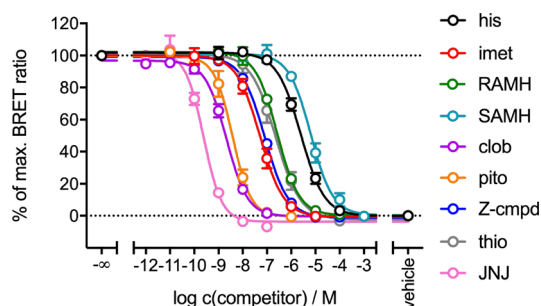


Figure 5. Displacement curves from BRET competition binding experiments of the fluorescent ligand **12** ($c = 500$ pM) and reported H_3 receptor ligands at HEK293 cells, stably expressing the NLuc- hH_3R . “Vehicle” denotes the condition where the cells were not incubated with **12**. Abbreviations used: histamine (his), imetit (imet), (R)-(-)- α -methylhistamine (RAMH), (S)-(+)- α -methylhistamine (SAMH), clobenpropit (clob), Z27743747 (Z-cmpd), thioperamide (thio), pitolisant (pito), and JNJ-5207852 (JNJ).

of 3 nM **12** in the imaging buffer with negligible background fluorescence (Figure 8A). We further tested the labeling efficiency under these conditions by using a H_3R control construct, which was C-terminally tagged with the photostable fluorescent protein mNeonGreen. Dual color acquisition revealed colocalization, a labeling efficiency of $96.1 \pm 2.1\%$, and a nonspecific binding of $2.5 \pm 0.8\%$ under these conditions (Figure 8B). Single-particle tracking of the acquired TIRF movies and subsequent diffusion analysis of the receptor tracks (Figure 8C,D) showed similar receptor dynamics for the H_3R (diffusion coefficient of $0.085 \pm 0.006 \mu m^2/s$) as shown previously for other class A GPCRs.^{50,51}

Table 3. Binding Data (pK_i Values) of Standard H_3R Ligands Determined at the Human H_3R in the NanoBRET Binding Assay^a

compound	NanoBRET UR-NR266 (12)		references	
	pK_i	N	pK_i	
his	6.23 ± 0.08	4	6.3; ⁴⁷ 6.5; ²³ 7.6; ⁴⁸ 8.0 ⁴⁵	
imet	7.90 ± 0.11	3	8.3; ⁴⁷ 8.8 ⁴⁵	
RAMH	7.20 ± 0.02	3	8.4; ⁴⁴ 8.2; ⁴⁵ 8.3 ⁴⁶	
SAMH	5.79 ± 0.11	3	6.4; ⁴⁷ 7.6; ⁴⁴ 7.2; ⁴⁵ 7.3 ⁴⁶	
clob	9.30 ± 0.08	3	9.6; ⁴⁷ 9.5; ²³ 8.6 ⁴⁵	
Z-cmpd	7.71 ± 0.01	3	7.4; ⁴² 7.3 ⁴⁶	
thio	7.28 ± 0.18	3	7.3; ⁴⁷ 7.4; ²³ 7.3 ⁴⁵	
pito	9.04 ± 0.12	3	8.6; ⁴⁷ 8.6 ⁴³	
JNJ	10.22 ± 0.02	3	9.2 ²⁵	

^aData represent mean values \pm SEM from N independent experiments, each performed in triplicate. NanoBRET experiments were performed at live HEK293 cells stably expressing the NLuc- hH_3R as described in the Experimental Section. The standard H_3R ligands used are depicted in Figure S4 in the Supporting Information. Abbreviations used: histamine (his), imetit (imet), (R)-(-)- α -methylhistamine (RAMH), (S)-(+)- α -methylhistamine (SAMH), clobenpropit (clob), Z27743747 (Z-cmpd), thioperamide (thio), pitolisant (pito), and JNJ-5207852 (JNJ).

Off-Target Studies. Once selectivity within the histamine receptor family was established, we sought to identify any binding of **12** to other GPCR groups. We performed an off-target screen using 14 different GPCRs. Therefore, we used the BRET-based binding assay with transient NLuc-receptor expression for our off-target screen. Unfortunately, the capacity

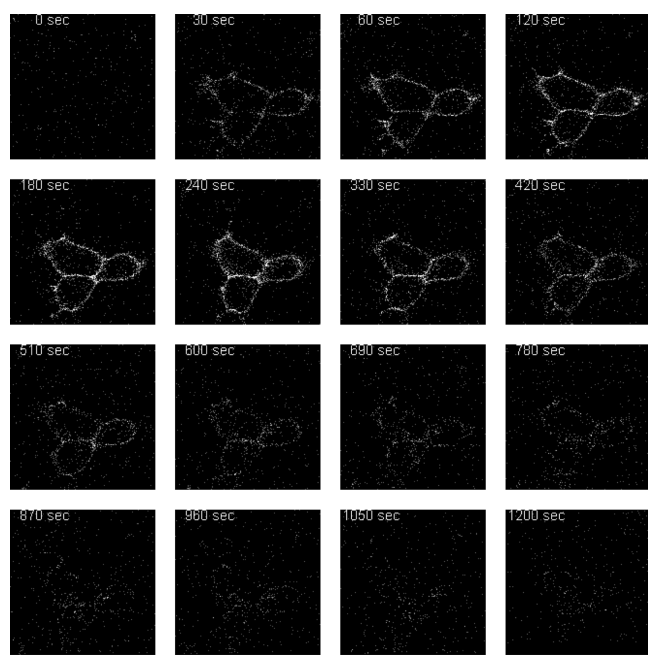


Figure 6. Time-lapse confocal microscopy images of the fluorescent ligand **12**: imaging of the HEK293-SP-FLAG-hH₃R cells treated with a 5 nM fluorescent ligand displayed a time-dependent increase of the fluorescence signal on the cell surface, indicating ligand binding to the H₃R. Competing **12** with the unlabeled H₃R antagonist clobenpropit decreased the fluorescence signal in a time-dependent manner (addition of clobenpropit after 220 s).

of the unpublished NLuc-receptor constructs to bind their endogenous ligands could not be thoroughly controlled given the lack of validated fluorescent ligands. Instead, it was only presumed based on sufficient surface expression of these constructs and based on the experience that N-terminal insertion of the NLuc usually does not affect the binding ability of class A GPCRs.^{15,52–55} Receptor cell surface expression was confirmed by an ELISA using a NanoLuc antibody (Cat. No. MAB100261, Bio-Techne, Minneapolis, MN, USA). Using 200 nM of **12**, we observed little off-target effects with only the muscarinic hM₂R and hM₄R displaying mild but significant response (13.2 ± 4.5 and $6.7 \pm 5.3\%$ of hH₃R response, respectively; **Figure 9**). Some ligand binding at the hM₂R and

hM₄R was unsurprising as the binding sites of these receptors share features with the hH₃R, and several characteristics of known H₃R ligands have been proven to be useful in developing muscarinic antagonists.^{56,57} It should be noted that BRET signals from binding experiments to different NLuc-GPCR constructs can only be compared with caution given the different N-terminal lengths and localizations of orthosteric binding pockets. Therefore, the low BRET signals observed at hM₂R and hM₄R (only $\sim 10\%$ of the BRET signal detected with NLuc-hH₃R) do not provide a quantitative value but rather an estimate for the binding of **12** to the receptors. Nevertheless, we believe that the low BRET signals for the muscarinic receptors using a maximal concentration of 200 nM do not indicate any off-target issues, as **12** has sub-nanomolar affinity for the target hH₃R.

CONCLUSIONS

In UR-NR266 (**12**), we described a sub-nanomolar affinity fluorescent ligand at the H₃R with an outstanding selectivity profile within the histamine receptor family. The TAMRA-labeled neutral antagonist was broadly characterized analytically and pharmacologically and showed excellent kinetic and fluorescence properties for further investigations. These results ensure excellent suitability for the recently described NanoBRET assay. The successful use as a fluorescent probe in the NanoBRET binding assay highlights the versatility of **12** and its suitability as a powerful tool in the urgently needed research for new drug candidates at the H₃R. A comprehensive off-target screening at 14 different receptors reveals **12** as a selective compound.

Due to its high affinity and exceptional receptor selectivity combined with high brightness and the proven low nonspecific binding, **12** shows remarkable results in fluorescence microscopy and is the first fluorescent ligand to enable single molecule imaging of the H₃R. Furthermore, it allows the presence of saturating concentrations in the imaging buffer during single-molecule image acquisition. This accounts for the obvious advantage of continuous labeling of receptors in the course of the experiment and compensates for potential fluorophore photobleaching. Thus, **12** is a versatile tool suitable for binding and also imaging studies at the H₃R. To the best of our knowledge, this is unique within the panel of available H₃R fluorescent ligands lifting the study of H₃R-

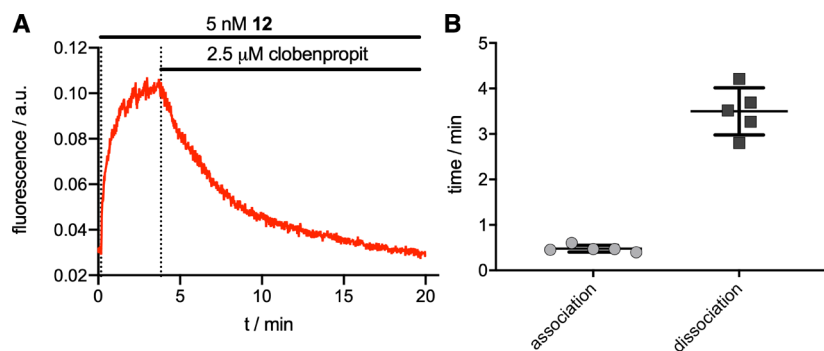


Figure 7. Association and dissociation kinetics of the fluorescent ligand: (A) representative graph displaying the quantification of the fluorescence signal obtained from experiments as in **Figure 1**. The fluorescence signal (in arbitrary units) was plotted as a function of time, and association/dissociation kinetics were calculated by fitting an exponential decay function on the signal (from baseline to saturation, and from saturation to decay to the baseline). Addition of the competitor clobenpropit after 220 s. (B) Scatter dot plot displaying the quantification of tau (τ) values for association/dissociation of the fluorescent ligand. Five cells from three independent experiments were analyzed. Data are represented as mean \pm SD.

Table 4. Kinetic Binding Constants of **12** at the Wild-Type hH₃R in Confocal Microscopy

compound	confocal microscopy					
	k_{obs}^a (min ⁻¹)	τ_{ass}^b (min)	k_{off}^a (min ⁻¹)	τ_{diss}^c (min)	k_{on}^d (min ⁻¹ nM ⁻¹)	$\text{p}K_{\text{d}}$ (kin) ^e
12	2.13 ± 0.14	0.48 ± 0.07	0.29 ± 0.02	3.50 ± 0.46	0.37 ± 0.03	9.10 ± 0.06

^aFive cells from three independent experiments were analyzed. Data represent mean values ± SEM. Confocal microscopy measurements performed at HEK293-SP-FLAG-hH₃R (wild-type hH₃R) cells. ^bFive cells from three independent experiments were analyzed. Data represent mean values ± CI (95%). Association time constant: $\tau_{\text{ass}} = 1/k_{\text{obs}}$. ^cFive cells from three independent experiments were analyzed. Data represent mean values ± CI (95%). Dissociation time constant: $\tau_{\text{diss}} = 1/k_{\text{off}}$. ^dAssociation rate constant: $k_{\text{on}} = (k_{\text{obs}} - k_{\text{off}})/c(\mathbf{12})$. Indicated errors were calculated according to the Gaussian law of error propagation. ^e K_{d} (kin) = $k_{\text{off}}/k_{\text{on}}$; $\text{p}K_{\text{d}}$ (kin) = $-\log K_{\text{d}}$ (kin). Indicated errors were calculated according to the Gaussian law of error propagation.

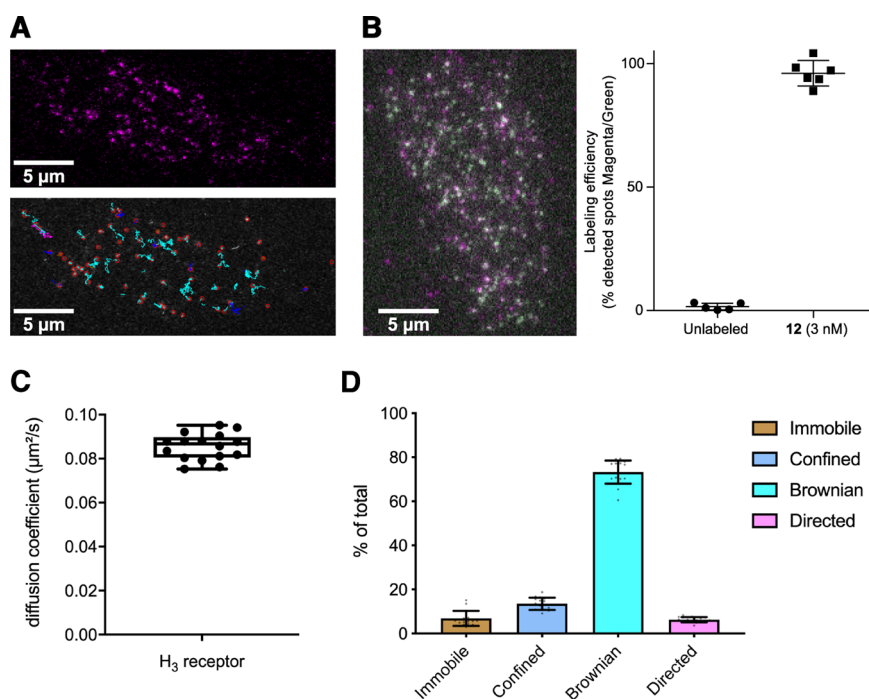


Figure 8. (A) Top panel: wild-type H₃ receptors labeled with 3 nM UR-NR266 (**12**). Bottom panel: single particle tracking of individual wild-type H₃ receptors and classification of diffusion classes (magenta = directed diffusion, blue = confined diffusion, cyan = Brownian motion, and brown = immobile). Shown images are representative of four independent experimental days. (B) Labeling efficiency measured by colocalization of the two colors in their corresponding detection channels (GFP/Cy3) as shown in the representative image. Labeling efficiencies are for the unlabeled control 2.5 ± 1.8 and 96.1 ± 5.2% at 3 nM **12**, respectively. Data are mean ± SD and originate from three independent experiments. Each data point refers to one cell. (C) Diffusion analysis based on single-particle tracking gives a diffusion coefficient of 0.085 ± 0.006 μm²/s. The diffusion type classification (D) is composed by 6.9 ± 0.8% immobile, 13.5 ± 0.7% confined, 73.3 ± 1.3% Brownian motion, and 6.3 ± 0.3% directed tracks undergoing the corresponding type of diffusion. Data are mean ± SD and originate from three independent experiments. Each data point refers to one cell.

dependent disease-related functions onto another level. Especially, the suitability in TIRF and confocal microscopy makes **12** a valuable tool to further investigate the role of the H₃R in the central nervous system, as the H₃R was reported to form heteroreceptor complexes in combination with other GPCRs and ion channels.^{7,9,10} This could be of great interest for research on neurodegenerative diseases, e.g., Alzheimer's disease, as these receptor complexes have arisen as promising targets to prevent neuronal cell death.¹⁰

EXPERIMENTAL SECTION

Chemistry. Commercially available chemicals (4-hydroxybenzaldehyde, 1-bromo-3-chloropropane, piperidine, sodium triacetoxyborohydride, ethyl isonipecotat, tetraethylene glycol, methanesulfonyl chloride, EDC, HOBt) and all other chemicals and solvents were purchased from standard commercial suppliers (Merck (Darmstadt, Germany), Sigma-Aldrich (Munich, Germany), Acros Organics (Geel, Belgium), Alfa Aesar (Karlsruhe, Germany), abcr (Karlsruhe,

Germany), or TCI Europe (Zwijndrecht, Belgium)) and were used as received. All solvents were of analytical grade. The syntheses of compounds **2–4** and **7–9** have already been described in the literature.^{25,26,33,58,59} The fluorescent dye 5-TAMRA NHS ester was purchased from Lumiprobe (Hannover, Germany). Deuterated solvents for nuclear magnetic resonance (¹H NMR and ¹³C NMR) spectra were purchased from Deutero GmbH (Kastellaun, Germany). All reactions carried out with dry solvents were accomplished in dry flasks under a nitrogen or argon atmosphere. For the preparation of buffers, HPLC eluents, and stock solutions, Millipore water was used. Column chromatography was accomplished using Merck silica gel Geduran 60 (0.063–0.200 mm) or Merck silica gel 60 (0.040–0.063 mm) (flash column chromatography). The reactions were monitored by thin layer chromatography (TLC) on Merck silica gel 60 F254 aluminum sheets, and spots were visualized under UV light at 254 nm by potassium permanganate or ninhydrin staining. Microwave assisted reactions were performed on an Initiator 2.0 synthesizer (Biotage, Uppsala, Sweden). Lyophilization was done with a Christ alpha 2–4 LD equipped with a Vacuubrand RZ 6 rotary vane vacuum pump. Nuclear magnetic resonance (¹H NMR and ¹³C NMR) spectra were

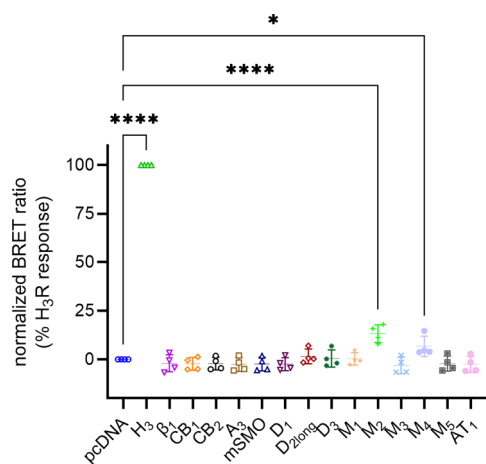


Figure 9. Off-target affinity in BRET binding experiments of the fluorescent ligand **12** ($c = 200$ nM) in HEK293T cells transiently expressing NLuc-receptor constructs. Data were normalized to the hH₃R (100%) and empty vector control (0%). Transfection with an empty pcDNA vector backbone is expressed as “pcDNA”. Receptor abbreviations are as follows: H₃, histamine H₃; β₁, β₁ adrenoceptor; CB_{1/2}, cannabinoid receptor type 1/2; A₃, adenosine A₃; mSMO, mouse smoothened; D_{1/2long/3r} dopamine D_{1/2long/3r}; M_{1/2/3/4/5r} muscarinic acetylcholine M_{1/2/3/4/5r}; AT₁, angiotensin II type 1. All receptor sequences are human, save the smoothened receptor originating from the mouse. Lines represent mean ± SD of four experiments, with each experimental condition performed in duplicate. Statistical significance was assessed by one-way ANOVA followed by Fisher’s LSD post-hoc test against “pcDNA”; *: $p < 0.05$; ****: $p < 0.0001$.

recorded on a Bruker (Karlsruhe, Germany) Avance 300 (¹H: 300 MHz, ¹³C: 75 MHz), 400 (¹H: 400 MHz, ¹³C: 101 MHz), or 600 (¹H: 600 MHz) spectrometer using perdeuterated solvents. The chemical shift δ is given in parts per million (ppm). Multiplicities were specified with the following abbreviations: s (singlet), d (doublet), t (triplet), q (quartet), quin (quintet), m (multiplet), and br (broad signal) as well as combinations thereof. ¹³C NMR-peaks were determined by DEPT 135 and DEPT 90 (distortionless enhancement by polarization transfer). NMR spectra were processed with MestReNova 11.0 (Mestrelab Research, Compostela, Spain). High-resolution mass spectrometry (HRMS) was performed on an Agilent 6540 UHD Accurate-Mass Q-TOF LC/MS system (Agilent Technologies, Santa Clara, CA) using an ESI source. Preparative HPLC was performed with a system from Waters (Milford, Massachusetts, USA) consisting of a 2524 binary gradient module, a 2489 detector, a prep inject injector, and a fraction collector III. A YMC-Triart C18 (150 × 20 mm, 5 μ m; YMC Co. Ltd., Kyoto, Japan) served as the stationary phase. As the mobile phase, 0.1% TFA in Millipore water and acetonitrile (MeCN) were used. The temperature was 25 °C, the flow rate was 20 mL/min, and UV detection was performed at 220 nm. Analytical HPLC experiments were performed on a 1100 HPLC system from Agilent Technologies equipped with an Instant Pilot controller, a G1312A Bin Pump, a G1329A ALS autosampler, a G1379A vacuum degasser, a G1316A column compartment, and a G1315B DAD detector. The column was a Phenomenex Kinetex XB-C18 column (250 × 4.6 mm, 5 μ m) (Phenomenex, Aschaffenburg, Germany), tempered at 30 °C. As the mobile phase, mixtures of MeCN and aqueous TFA were used (linear gradient: MeCN/TFA (0.1%) (v/v) 0 min: 10:90, 25–35 min: 95:5, 36–45 min: 10:90; flow rate = 1.00 mL/min, $t_0 = 3.21$ min). Capacity factors were calculated according to $k = (t_R - t_0)/t_0$. Detection was performed at 220 nm. Furthermore, filtration of the stock solutions with PTFE filters (25 mm, 0.2 μ m, Phenomenex Ltd., Aschaffenburg, Germany) was carried out before testing. Compound purities determined by HPLC were calculated as the peak area of the

analyzed compound in % relative to the total peak area (UV detection at 220 nm). The HPLC purity (see Figure S1, SI) of the final compound **12** was 99%. The tested compound **12** has been screened for PAINS and aggregation by publicly available filters (<http://zinc15.docking.org/patterns/home>, <http://advisor.docking.org>).^{60,61} The compound has not been previously reported as PAINS or an aggregator. None of the data showed abnormalities, e.g., high Hill slopes, what could be a hint for PAINS.⁶¹

Synthesis and Analytical Data. **4-(3-Chloropropoxy)-benzaldehyde (2).**²⁵ A suspension of 4-hydroxybenzaldehyde (5.00 g, 40.94 mmol, 1 eq), 1-bromo-3-chloropropane (8.06 mL, 81.88 mmol, 2 eq), and K₂CO₃ (16.85 g, 121.92 mmol, 3 eq) in MeCN was heated to reflux for 18 h. After cooling to room temperature, the solid was filtered off and the filtrate was dried in vacuo. The resulting residue was dissolved in EtOAc and washed with water and brine and dried over Na₂SO₄, and the solvent was removed under reduced pressure. The crude product was purified by column chromatography (PE/EtOAc 9:1). **2** (7.26 g, 89%) was obtained as a yellow oil. $R_f = 0.40$ (PE/EtOAc 8:1). ¹H NMR (300 MHz, CDCl₃) δ 9.89 (s, 1H), 7.95–7.75 (m, 2H), 7.09–6.91 (m, 2H), 4.21 (t, $J = 5.9$ Hz, 2H), 3.76 (t, $J = 6.2$ Hz, 2H), 2.36–2.18 (m, 2H). ¹³C NMR (75 MHz, CDCl₃) δ 190.8, 163.7, 132.0, 130.1, 114.8, 64.6, 41.2, 32.0. HRMS (ESI-MS): m/z [M + H⁺] calculated for C₁₀H₁₂ClO₂⁺: 199.0520, found 199.0516; C₁₀H₁₁ClO₂ (198.65).

4-(3-(Piperidin-1-yl)propoxy)benzaldehyde (3).²⁵ **2** (7.22 g, 36.34 mmol, 1 eq), piperidine (5.38 mL, 54.51 mmol, 1.5 eq), Na₂CO₃ (5.78 g, 54.51 mmol, 1.5 eq), and KI (0.30 g, 1.82 mmol, 5 mol %) were heated to reflux in MeCN for 20 h. The solvent was removed under reduced pressure, and the residue was dissolved in DCM. The organic phase was washed with water and brine and dried over Na₂SO₄, and the solvent was removed under reduced pressure. Column chromatography (DCM/MeOH 9/1 + 0.1% NEt₃) afforded **3** (6.79 g, 76%) as a yellow oil. $R_f = 0.48$ (DCM/MeOH/7 N NH₃ in MeOH 95:4:1). ¹H NMR (400 MHz, CDCl₃) δ 9.87 (s, 1H), 7.88–7.74 (m, 2H), 7.06–6.92 (m, 2H), 4.09 (t, $J = 6.4$ Hz, 2H), 2.51–2.31 (m, 6H), 2.06–1.94 (m, 2H), 1.63–1.54 (m, 4H), 1.50–1.38 (m, 2H). ¹³C NMR (101 MHz, CDCl₃) δ 190.8, 164.2, 132.0, 129.8, 114.8, 66.9, 55.7, 54.7, 26.7, 26.0, 24.4. HRMS (ESI-MS): m/z [M + H⁺] calculated for C₁₅H₂₂NO₂⁺: 248.1645, found 248.1673; C₁₅H₂₁NO₂ (247.34).

Ethyl 1-(4-(3-(Piperidin-1-yl)propoxy)benzyl)piperidine-4-carboxylate (4).²⁶ Sodium triacetoxyborohydride (5.35 g, 25.23 mmol, 1.3 eq) was added to a solution of **3** (4.80 g, 19.41 mmol, 1 eq) and ethyl isonipecotatate (3.29 mL, 21.35 mmol, 1.1 eq) in CHCl₃ at room temperature, and the reaction was stirred for 20 h. A saturated solution of sodium bicarbonate was added, and the organic phase was separated. The aqueous phase was extracted with DCM, the combined organic phases were washed with brine and dried over Na₂SO₄, and the solvent was removed under reduced pressure. Column chromatography (DCM/MeOH 95/5 + 0.1% NH₃) afforded **4** (7.18 g, 95%) as a yellow oil. $R_f = 0.28$ (DCM/MeOH/7 N NH₃ in MeOH 95:4:1). ¹H NMR (300 MHz, CDCl₃) δ 7.22–7.16 (m, 2H), 6.87–6.78 (m, 2H), 4.12 (q, $J = 7.1$ Hz, 2H), 3.99 (t, $J = 6.4$ Hz, 2H), 3.41 (s, 2H), 2.83 (d, $J = 11.6$ Hz, 2H), 2.53–2.36 (m, 6H), 2.32–2.18 (m, 1H), 2.05–1.90 (m, 4H), 1.91–1.68 (m, 4H), 1.65–1.54 (m, 4H), 1.50–1.39 (m, 2H), 1.24 (t, $J = 7.1$ Hz, 3H). ¹³C NMR (75 MHz, CDCl₃) δ 175.3, 158.1, 130.3, 114.2, 66.5, 62.7, 60.3, 56.1, 54.6, 52.8, 41.3, 28.3, 26.8, 25.9, 24.4, 14.2. HRMS (ESI-MS): m/z [M + H⁺] calculated for C₂₃H₃₇N₂O₃⁺: 389.2799, found 389.2800; C₂₃H₃₆N₂O₃ (388.55).

1-(4-(3-(Piperidin-1-yl)propoxy)benzyl)piperidine-4-carboxylic Acid Dihydrochloride (5).²⁶ 2 N aqueous HCl was added to a solution of **4** (2.06 g, 5.30 mmol, 1 eq) in THF and stirred at room temperature overnight. The solvent was evaporated, and the product was dried in vacuo. A sticky brown oil was obtained (**5**, 2.10 g, 92%). ¹H NMR (300 MHz, CD₃OD) δ 7.55–7.47 (m, 2H), 7.07–6.98 (m, 2H), 4.27 (s, 2H), 4.14 (t, $J = 5.8$ Hz, 2H), 3.64–3.44 (m, 4H), 3.14–2.92 (m, 4H), 2.72–2.57 (m, 1H), 2.34–1.77 (m, 12H). ¹³C NMR (101 MHz, CD₃OD) δ 173.6, 159.9, 132.8, 121.2, 114.8, 64.9, 59.7, 54.4, 53.1, 51.0, 38.2, 25.3, 23.8, 22.9, 21.3. HRMS (ESI-MS):

m/z $[M + H^+]$ calculated for $C_{21}H_{33}N_2O_3^+$: 361.2486, found 361.2490; $C_{21}H_{32}N_2O_3 \times 2 HCl$ (433.42).

(*Oxybis(ethane-2,1-diy)bis(oxy)bis(ethane-2,1-diy) Dimethanesulfonate (7)*).⁵⁸ Triethylamine (43.06 mL, 308.92 mmol, 6 eq) was added at 0 °C to a solution of tetraethylene glycol (**6**, 10.00 g, 51.49 mmol, 1 eq) and methanesulfonyl chloride (17.69 g, 154.46 mmol, 3 eq) in DCM, and the reaction was stirred at room temperature for 20 h. Water was added, and the organic phase was separated, washed with brine, and dried over Na_2SO_4 , and the solvent was removed under reduced pressure. Column chromatography (DCM/MeOH 98/2) afforded **7** (14.03 g, 78%) as a slightly yellow oil. R_f = 0.70 (DCM/MeOH 95:5). 1H NMR (300 MHz, $CDCl_3$) δ 4.42–4.29 (m, 4H), 3.80–3.70 (m, 4H), 3.69–3.57 (m, 8H), 3.06 (s, 6H). ^{13}C NMR (75 MHz, $CDCl_3$) δ 70.6, 70.5, 69.3, 69.0, 37.7. HRMS (ESI-MS): m/z $[M + H^+]$ calculated for $C_{10}H_{23}O_9S_2^+$: 351.0778, found 351.0783; $C_{10}H_{22}O_9S_2$ (350.40).

1-Azido-2-(2-(2-(2-azidoethoxy)ethoxy)ethoxy)ethane (8).³³ **7** (5.00 g, 14.27 g, 1 eq) and sodium azide (3.71 g, 57.08 mmol, 4 eq) were dissolved in EtOH/DMF (4/1) and heated to reflux for 20 h. The solvent was removed under reduced pressure, the residue was dissolved in Et_2O , the organic phase was washed subsequently with water and saturated ammonium chloride solution and dried over Na_2SO_4 , and the solvent was removed under reduced pressure. The product was dried *in vacuo*. A colorless oil was obtained for **8** (3.14 g, 90%). 1H NMR (300 MHz, $CDCl_3$) δ 3.71–3.62 (m, 12H), 3.43–3.33 (m, 4H). ^{13}C NMR (75 MHz, $CDCl_3$) δ 70.7, 70.1, 50.7. HRMS (ESI-MS): m/z $[M + H^+]$ calculated for $C_8H_{17}N_6O_3^+$: 245.1357, found 245.1359; $C_8H_{16}N_6O_3$ (244.26).

2-(2-(2-(2-Azidoethoxy)ethoxy)ethoxy)ethan-1-amine (9).⁵⁹ **8** (2.00 g, 8.19 mmol, 1 eq) was dissolved in a mixture of 1 N aqueous HCl, THF, and EtOAc (5/1/5 v/v/v). Triphenylphosphine (2.14 g, 8.19 mmol, 1 eq) in EtOAc was added slowly at room temperature, and the reaction was stirred overnight. The reaction was basified with aqueous NaOH solution, the solvent was removed under reduced pressure, and the crude product was purified by column chromatography (DCM/MeOH 95/5 + 0.1% NH_3). A slightly yellow oil was obtained for **9** (1.37 g, 77%). R_f = 0.32 (DCM/MeOH/7 N NH_3 in MeOH 95:4:1). 1H NMR (300 MHz, $CDCl_3$) δ 3.70–3.59 (m, 12H), 3.40 (m, 2H), 3.04 (t, J = 5.0 Hz, 2H). ^{13}C NMR (75 MHz, $CDCl_3$) δ 70.5, 70.4, 70.1, 69.9, 69.4, 50.7, 40.4. HRMS (ESI-MS): m/z $[M + H^+]$ calculated for $C_8H_{19}N_4O_3^+$: 219.1452, found 219.1453; $C_8H_{18}N_4O_3$ (218.26).

N-(2-(2-Azidoethoxy)ethyl)-1-(4-(3-(piperidin-1-yl)propoxy)benzyl)piperidine-4-carboxamide (10). **5** (100 mg, 0.23 mmol, 1 eq), 1-ethyl-3-(3-dimethylaminopropyl)carbodiimide (48 mg, 0.25 mmol, 1.1 eq), 1-hydroxybenzotriazole (34 mg, 0.25 mmol, 1.1 eq), and DIPEA (119 mg, 0.92 mmol, 4 eq) were dissolved in DMF/DCM (1/1) in a microwave vial and stirred at room temperature for 30 min. **9** (50 mg, 0.23 mmol, 1 eq) was added, and the reaction was stirred 30 min at 100 °C in a microwave reactor (sealed vial). The solvent was removed under reduced pressure, and the crude product was purified by column chromatography (DCM/MeOH 95/5 + 0.1% NH_3). A brown oil was obtained for **10** (85 mg, 65%). R_f = 0.36 (DCM/MeOH/7 N NH_3 in MeOH 90:9:1). 1H NMR (300 MHz, $CDCl_3$) δ 7.20–7.12 (m, 2H), 6.84–6.75 (m, 2H), 6.08 (t, J = 5.2 Hz, 1H), 3.95 (t, J = 6.4 Hz, 2H), 3.66–3.55 (m, 10H), 3.53–3.46 (m, 2H), 3.37 (m, 6H), 2.87 (m, 2H), 2.50–2.30 (m, 6H), 2.13–1.84 (m, 5H), 1.73 (m, 4H), 1.56 (m, 4H), 1.47–1.33 (m, 2H). ^{13}C NMR (101 MHz, $CDCl_3$) δ 175.1, 158.1, 130.2, 130.2, 114.1, 70.7, 70.6, 70.6, 70.2, 70.1, 69.9, 66.5, 62.6, 56.0, 54.6, 53.0, 50.7, 43.4, 39.0, 28.9, 26.8, 25.9, 24.4. HRMS (ESI-MS): m/z $[M + H^+]$ calculated for $C_{29}H_{49}N_6O_5^+$: 561.3759, found 561.3767; $C_{29}H_{48}N_6O_5$ (560.74).

N-(2-(2-Aminoethoxy)ethyl)-1-(4-(3-(piperidin-1-yl)propoxy)benzyl)piperidine-4-carboxamide (11). Triphenylphosphine (60 mg, 0.23 mmol, 1.5 eq) was added to a solution of **10** (85 mg, 0.15 mmol, 1 eq) in THF, and the reaction was stirred for 4 h at 45 °C. Water was added, and the reaction was stirred for another 2 h at the same temperature. THF was removed under reduced pressure, and trifluoroacetic acid (200 μ L) was added to the aqueous solution. The crude product was purified by preparative HPLC. A colorless oil

was obtained for **11** (79 mg, 60%). R_f = 0.22 (DCM/MeOH/7 N NH_3 in MeOH 90:9:1). 1H NMR (400 MHz, DMSO- d_6) δ 10.05–9.65 (m, 2H), 8.04 (t, J = 5.4 Hz, 1H), 7.90 (br s, 3H), 7.45–7.37 (m, 2H), 7.06–6.93 (m, 2H), 4.27–4.26 (m, 2H), 4.06 (t, J = 5.9 Hz, 2H), 3.66–3.43 (m, 12H), 3.42–3.28 (m, 4H), 3.26–3.13 (m, 4H), 3.02–2.75 (m, 6H), 2.42–2.29 (m, 1H), 2.20–2.05 (m, 2H), 1.92–1.54 (m, 9H), 1.46–1.28 (m, 1H). ^{13}C NMR (101 MHz, DMSO- d_6) δ 173.3, 159.5, 159.0, 158.7, 133.3, 122.2, 118.5, 115.6, 115.1, 70.2, 70.1, 70.1, 70.0, 69.4, 67.1, 65.5, 59.0, 53.8, 52.6, 51.0, 39.0, 38.9, 26.2, 23.9, 23.0, 21.7. HRMS (ESI-MS): m/z $[M + H^+]$ calculated for $C_{29}H_{51}N_4O_5^+$: 535.3854, found 535.3855; $C_{29}H_{50}N_4O_5 \times 3 TFA$ (876.81).

2-(6-(Dimethylamino)-3-(dimethyliminio)-3H-xanthen-9-yl)-5-((1-oxo-1-(1-(4-(3-(piperidin-1-yl)propoxy)benzyl)piperidin-4-yl)-5,8,11-trioxo-2-azatridecan-13-yl)carbonyl)benzoate Dihydrotrifluoroacetate (12). **11** (7.89 mg, 9 μ mol, 1.5 eq) was dissolved in DMF (30 μ L). NEt_3 (6.68 mg, 66 μ mol, 11 eq) and 5-carboxytetramethylrhodamine succinimidyl ester (5-TAMRA NHS ester) (3.17 mg, 6 μ mol, 1 eq) in DMF (60 μ L) were added, and the reaction was shaken for 2.5 h in the dark at room temperature. The reaction was quenched with 10% aqueous TFA (20 μ L), and the crude product was purified by preparative HPLC. A pink solid was obtained for **12** (5.7 mg, 4.9 μ mol, 82%). RP-HPLC: 99%, (t_R = 9.84 min, k = 2.07). 1H NMR (600 MHz, DMSO- d_6) δ 9.84–9.57 (m, 1H), 9.48 (br s, 1H), 8.95 (t, J = 5.5 Hz, 1H), 8.65 (br s, 1H), 8.28 (d, J = 7.9 Hz, 1H), 8.01 (t, J = 5.7 Hz, 1H), 7.54 (br s, 1H), 7.45–7.38 (m, 2H), 7.10–6.97 (m, 4H), 6.94 (br s, 2H), 6.56 (br s, 2H), 4.20 (s, 2H), 4.05 (t, J = 6.0 Hz, 2H), 3.64–3.43 (m, 18H), 3.29–3.04 (m, 16H), 2.94–2.82 (m, 4H), 2.39–2.32 (m, 1H), 2.18–2.08 (m, 2H), 2.04–1.60 (m, 9H), 1.45–1.31 (m, 1H). HRMS (ESI-MS): m/z $[M + H^+]$ calculated for $C_{54}H_{71}N_6O_9^+$: 947.5277, found 947.5293; $C_{54}H_{70}N_6O_9 \times 2 TFA$ (1175.23).

Fluorescence Properties. Excitation and emission spectra of **12** were recorded in PBS (137 mM NaCl, 2.7 mM KCl, 10 mM Na_2HPO_4 , 1.8 mM KH_2PO_4 , pH 7.4) containing 1% BSA (Sigma-Aldrich, Munich, Germany) using a Cary Eclipse spectrofluorometer (Varian Inc., Mulgrave, Victoria, Australia) at 22 °C, in acryl cuvettes (10 \times 10 mm, Sarstedt, Nümbrecht, Germany). The slit adjustments (excitation/emission) were 5/10 nm for excitation spectra and 10/5 nm for emission spectra. Net spectra were calculated by subtracting the respective vehicle reference spectrum, and corrected emission spectra were calculated by multiplying the net emission spectra with the respective lamp correction spectrum. The quantum yield of **12** was determined according to previously described procedures^{23,62} with minor modifications using a Cary Eclipse spectrofluorometer (Varian Inc., Mulgrave, Victoria, Australia) at 22 °C, using acryl cuvettes (10 \times 10 mm, Sarstedt, Nümbrecht, Germany) and cresyl violet perchlorate (Biomol GmbH – Life Science Shop, Hamburg, Germany) as a red fluorescent standard. Absorption spectra were recorded by UV/Vis spectroscopy (350–850 nm, scan rate: 300 nm/min, slits: fixed 2 nm) at a concentration of 2 μ M for cresyl violet (in EtOH, $\lambda_{abs,max}$ = 575 nm) and **12** (in PBS buffer and PBS + 1% BSA, $\lambda_{abs,max}$ = 550 nm). The quantum yields were calculated for three different slit adjustments (exc./em.): 5/5, 10/5, and 10/10 nm. The means of the quantum yields, absorption and emission maxima, and absorbance are presented in Table S1 in the Supporting Information.

BRET-Based Saturation/Real-Time Kinetics/Competition Binding at the NLuc-H₃R. BRET-based saturation/real-time kinetics/competition binding at the NLuc-H₃R were performed as previously described by Bartole et al. with minor modifications.²³ For the determination of nonspecific binding, clobenpropit (500-fold excess) was used instead of thioperamide. Dissociation was initiated by addition of 250 nM clobenpropit (500-fold excess) instead of thioperamide. For competition binding experiments, **12** was used in a concentration of 500 pM. Histamine dihydrochloride (his) was from TCI Chemicals (Tokyo, Japan). Imetit dihydrobromide (imet), (R)-(-)- α -methylhistamine dihydrobromide (RAMH), (S)-(+)- α -methylhistamine dihydrobromide (SAMH), clobenpropit dihydrobromide (clob), and thioperamide maleate (thio) were from Tocris Bioscience (Ellisville, MO, USA). Z27743747 (Z-cmpd) was from Enamine Ltd.

(Kyiv, Ukraine). Pitolisant hydrochloride (pito) was kindly provided by Prof. Dr. Katarzyna Kiec-Kononowicz (Jagiellonian University, Krakow). Significant differences between pK_d values were assessed using a two-tailed *t*-test ($p < 0.05$).

Flow Cytometry. Flow cytometric saturation binding experiments at the H_3 receptor were performed with a FACSCanto II flow cytometer (Becton Dickinson, Heidelberg, Germany) equipped with an argon laser (488 nm) and a red diode laser (640 and 635 nm). Fluorescence signals were recorded using the following instrument settings: excitation: 488 nm, emission: 585 ± 21 nm (PE channel). All samples were prepared and incubated in 1.5 mL cups (Eppendorf, Hamburg, Germany). Cells were seeded 5 to 6 days prior to the experiment in cell culture flasks. On the day of the experiment, the cells were treated with trypsin/EDTA (0.05%/0.02%) (Sigma-Aldrich, Munich, Germany), detached, and suspended in the cell culture medium followed by centrifugation. The cells were resuspended in Leibovitz's L-15 medium (Fisher Scientific, Nidderau, Germany) with 1% BSA (in the following, referred to as L-15 medium). The cell density was adjusted to 100,000 cells/mL. For the total binding experiments, 2.5 μ L of a solution of the fluorescent ligand (100-fold concentrated to final concentration) in the L-15 medium and 2.5 μ L of L-15 medium were added to 245 μ L of the cell suspension. For the nonspecific binding experiments, 2.5 μ L of solution of the fluorescent ligand (100-fold concentrated to final concentration) and 2.5 μ L of a 1 mM solution of clobenpropit in the L-15 medium were added to 245 μ L of the cell suspension. NR266 (**12**) was used at final concentrations of 0.02–10 nM. All samples were incubated at 22 °C in the dark under shaking for 1 h. All experiments were performed in duplicate.

Radioligand Competition Binding. Radioligand competition binding experiments were performed as previously described by Pockes et al. with minor modifications.⁴⁸ All experiments were carried out on whole HEK cells instead of Sf9 membranes. Generation of the stable HEK293-SP-FLAG-hH₁R and HEK293-SP-FLAG-hH₃R cell lines was conducted as described for the HEK293-SP-FLAG-hH₃R and HEK293-SP-FLAG-hH₁R.²³ Ligand dilutions of **12** were prepared 10-fold concentrated in L-15 with 1% BSA, and 10 μ L/well was transferred to a flat-bottom polypropylene 96-well microtiter plate (Greiner Bio-One, Frickenhausen, Germany), as well as 10 μ L/well of the respective radioligand. The cells were adjusted to a density of 1.25×10^6 cells/mL, and 80 μ L of the cell suspension was added to each well (total volume of 100 μ L). All data were analyzed using GraphPad Prism8 software (San Diego, CA, USA). The normalized competition binding curves were then fitted with a four-parameter logistic fit yielding pIC_{50} -values. These were transformed into pK_i -values using the Cheng–Prusoff equation.⁶³

BRET Measurements of Ligand-Induced G₁₂ Activation. The G₁₂ BRET sensor was generated as previously described.³⁷ For the BRET measurements, HEK293A cells were transiently transfected in a suspension with wild-type H₃R and G₁₂ BRET sensor (1:1 plasmid ratio) using Lipofectamine 2000 (Thermo Fisher Scientific, Nidderau, Germany) (2 μ L transfection reagent/ μ g total plasmid) and seeded onto poly-D-lysine-precoated, white 96-well plates (Greiner Bio-One, Frickenhausen, Germany) (30,000 cells/well). 48 h after transfection, cells were washed with HBSS (Gibco/Life Technologies, Carlsbad, USA) and incubated with a 1/1000 stock solution of furimazine (Promega, Mannheim, Germany). 5 min later, baseline BRET was recorded in three consecutive reads (4 min), 10-fold serial ligand dilutions or vehicle control was added, and the ligand-induced BRET ratio was recorded in 17 consecutive reads (36 min). For competition experiments, cells grown in 96-well plates were washed 48 h after transfection as described above and incubated with a 1/1000 stock solution of furimazine along with the indicated concentrations of compound **12** or ultrapure water (solvent control). After recording the basal BRET ratio, all wells pre-incubated with **12** were stimulated with 1 nM imetit. Wells pre-incubated with ultrapure water were treated with HBSS (vehicle control for imetit treatment). All experiments were conducted using a CLARIOstar plate reader (BMG Labtech, Ortenberg, Germany) recording NLuc and cpVenus emission intensities with 450/80 nm (Gain 3600) and 530/30 nm

(Gain 4000) monochromator settings, respectively, and an integration time of 0.3 s. Raw BRET ratios were defined as acceptor emission/donor emission. The three BRET ratios prior to ligand/vehicle addition were averaged and defined as BRET_{basal}. To quantify ligand-induced BRET changes, Δ BRET was calculated for each well and time point as a percent over basal ($[(BRET_{stim} - BRET_{basal})/BRET_{basal}] \times 100$). Subsequently, the average Δ BRET of vehicle-treated control wells was subtracted. Ligand concentration response curves were generated based on vehicle-corrected Δ BRET measured as a mean of three subsequent reads, 23 min after ligand addition.

Live Cell Confocal Microscopy. HEK293 cells stably transfected with a vector plasmid for H₃R expression were maintained in Dulbecco's Modified Eagle's Medium (DMEM) (PAN Biotech, Aidenbach, Germany) supplemented with 10% Fetal Bovine Serum (FBS) (PAN, Aidenbach, Germany Biotech), 1% L-Glutamine (PAN Biotech, Aidenbach, Germany), penicillin (100 U/mL), and streptomycin (100 μ g/mL) at 37 °C and 5% CO₂. Cells were passaged every 2–3 days.

For imaging, 300,000 HEK293-H₃R cells were seeded on poly-D-lysine coated coverslips in 6-well plates. 24 h later, coverslips were transferred to an Attofluor cell chamber (Thermo Fisher Scientific, Nidderau, Germany) and supplemented with Fluorobrite DMEM medium (Thermo Fisher, Nidderau, Germany), and then the chamber was placed on a microscope stage.

Imaging was performed using a Leica SP8 laser scanning confocal microscope equipped with a 40 \times /1.25 NA oil immersion objective, a white light laser (WLL), and photon counting hybrid (HyD) detectors. For excitation, the WLL was set to 552 nm at 10% power. Fluorescence was detected within an emission window of 557–764 nm. Image size was set to 512 \times 512 pixels, and the scanning speed was 700 Hz. After adjusting the focus, time-lapse cell imaging was performed with a 1 s interval between each image. After imaging for 10 s of baseline, the fluorescent ligand was added by using a micropipette at a final concentration of 5 nM. After imaging for 4–5 min, clobenpropit was added at a final concentration of 2.5 μ M, maintaining the 5 nM fluorescent ligand concentration, and imaging was completed after 20 min.

Time-lapse confocal images were processed using the ImageJ software. Contrast was adjusted for each file to facilitate the visualization of the fluorescence signal. Total fluorescence (in arbitrary units) was plotted as a function of time using the Origin 2018 software. Association and dissociation kinetics were calculated using the “ExpDec” function in the software. Each kinetic data was pooled and plotted as a scatter dot-plot using the GraphPad 7 software.

Experiments to demonstrate the photobleaching properties were performed according to the method described above. The fluorescent ligand was immobilized in a 0.5% agarose film in 1 μ M final concentration of the fluorescent ligand UR-NR266 (**12**) and imaged over a period of 20 min.

TIRF-Imaging. For single-molecule experiments, CHO-cells (ATTC/LGC Standards, Wesel, Germany) were seeded 24 h before transfection. Transfection was done 4–6 h before TIRF-imaging using Lipofectamine 2000 (Thermo Fisher Scientific, Nidderau, Germany). For each single well of a 6-well cell culture plate (Brand, Wertheim, Germany), 2 μ g of the desired DNA was diluted in 500 μ L of Opti-MEM (Thermo Fisher Scientific, Nidderau, Germany) and mixed with another dilution containing 6 μ L of Lipofectamine 2000 transfection reagent in 500 μ L of Opti-MEM. After incubation at 25 °C for 20 min, this mixture (total = 1 mL) was added to a single well of cell culture plate, containing 1 mL of DMEM-F12 medium (Thermo Fisher Scientific, Nidderau, Germany). After 4–6 h, expression levels were sufficient for single-molecule experiments and the medium was exchanged with a new DMEM-F12 medium.

All TIRF-imaging experiments were performed with transiently transfected CHO cells as described above. To measure the labeling efficiency of UR-NR-266 (**12**), a C-terminally mNeonGreen tagged H₃R was expressed (H3-mNG). Cells were labeled with 10 nM of **12** for 15 min. After labeling, cells were washed once with PBS and taken for imaging to an Attofluor Cell Chamber (Invitrogen, Carlsbad,

USA) in sterile filtered PBS (Sigma-Aldrich, Munich, Germany) containing 3 nM **12**. For single-molecule imaging, a TIRF illuminated Nikon Eclipse Ti2 microscope (Nikon, Tokyo, Japan) equipped with a 100× 1.49NA automated correction collar objective and 405, 488, 561, and 647 nm laser diodes coupled via an automated N-Storm module and four iXon Ultra 897 EMCCD cameras (Andor, Tokyo, Japan) was used. The objective and sample were kept at 20 °C during imaging. The automated objective collar was on, exposure times were set to 40 ms, and the perfect focus system (Nikon, Tokyo, Japan) was activated. Emission of TAMRA was recorded using a Cy3 Filter (Chroma, Vermont, USA), and mNeonGreen was recorded using a GFP Filter (Chroma, Vermont, USA).

Image analysis of the obtained TIRF-movies was done by first cropping the image to the desired size, region, and frame-number using Fiji.⁶⁴ Afterward, movies were loaded in the Matlab environment (MathWorks) using u-Track,⁶⁵ and requested parameters were adjusted according to the abovementioned imaging conditions. Spot-Detection, Tracking, and Motion-Analysis modules were then applied and analyzed as previously described, as well as the assignment of diffusion classes.^{51,66}

Off-Target Screening Using the NanoBRET Binding Assay.

The NLuc construct of the mouse smoothened receptor⁵³ was kindly provided by Prof. Dr. Gunnar Schulte (Karolinska Institutet), the adenosine A₃ receptor¹⁵ by Prof. Dr. Stephen J. Hill (University of Nottingham), the β₁ adrenoceptor by Dr. Ulrike Zabel (University of Würzburg), the muscarinic acetylcholine M₂ receptor⁵⁴ by Dr. Lukas Grätz (University of Regensburg), and the dopamine D₁ receptor by Denise Mönnich (University of Regensburg). All other constructs were made for these purposes by Dr. Lukas Grätz and Dr. Hannes Schihada. For the BRET-based off-target screening, HEK293T cells were transiently transfected in a suspension with 1 μg of cDNA per mL of cell suspension (300,000 cells/mL). The receptors were the histamine H₃, β₁ adrenoceptor, cannabinoid receptor types 1 and 2, adenosine A₃, mouse smoothened, dopamine D_{1/2long/3}, muscarinic acetylcholine M_{1/2/3/4/5}, and angiotensin II type 1 receptor and were prepared by replacing the receptor sequence of the NLuc-A₃ construct. After 5 min of incubation, the mixtures were combined and incubated at room temperature for a further 10 min. HEK293T cells were suspended at 300,000 cells/mL in DMEM (10% FCS), and 1 mL of cell suspension was added to each receptor/PEI mix. Seeding consisted of 100 μL of cDNA/cell/PEI mixture per well on a poly-D-lysine (mol wt 70,000–150,000, Sigma-Aldrich, Taufkirchen, Germany) coated white 96 well plate (cellGrade, Brand, Wertheim, Germany). Cells were used 36 h after transfection. Media was aspirated and washed with HBSS/0.5% BSA, before being replaced with 90 μL of HBSS/0.5% BSA plus flurimazine (1:1000 dilution) and incubated for 5 min at 37 °C. Bioluminescence and fluorescence were read on the Tecan GENios Pro, using the same parameters as the other BRET experiments at 37 °C. The baseline was read for 5 cycles, and the response post ligand addition was read for another 10 min. Buffer control and 200 nM **12** were used in duplicate for each receptor.

■ ASSOCIATED CONTENT

Supporting Information

The Supporting Information is available free of charge at <https://pubs.acs.org/doi/10.1021/acs.jmedchem.1c01089>.

Chemical stability (Figure S1), fluorescence properties (Figure S2, Table S1), imetit-induced G₁₂ activation (Figure S3), structures of competitive histamine receptor ligands (Figure S4), kinetic binding data from confocal microscopy (Figure S5), supplementary data from TIRF microscopy (Figure S6), synthesis of 1-[4-(3-piperidin-1-ylpropoxy)benzyl]piperidine (JNJ-5207852) (Scheme S1), NMR spectra (Figures S7–S26), live cell ELISA for surface expression (Figure S27), photobleaching (Figure S28) (PDF)
Molecular Formula Strings (CSV)

Single-molecule imaging (AVI)

Single-particle tracking (AVI)

■ AUTHOR INFORMATION

Corresponding Authors

Lukas Grätz – Institute of Pharmacy, University of Regensburg, Regensburg 93053, Germany;

Email: lukas.graetz@ur.de

Steffen Pockes – Institute of Pharmacy, University of Regensburg, Regensburg 93053, Germany; Department of Neurology, University of Minnesota, Minneapolis, Minnesota 55455, United States; Department of Medicinal Chemistry, Institute for Therapeutics Discovery and Development, University of Minnesota, Minneapolis, Minnesota 55414, United States; orcid.org/0000-0002-2211-9868;
Email: steffen.pockes@ur.de

Authors

Niklas Rosier – Institute of Pharmacy, University of Regensburg, Regensburg 93053, Germany

Hannes Schihada – Section of Receptor Biology & Signaling, Dept. of Physiology & Pharmacology, Karolinska Institutet, Stockholm 171 77, Sweden; orcid.org/0000-0002-1889-1636

Jan Möller – Max Delbrück Center for Molecular Medicine, Berlin 13125, Germany; Institute of Pharmacology and Toxicology and Rudolf Virchow Center, University of Würzburg, Würzburg 97070, Germany

Ali İşbilir – Max Delbrück Center for Molecular Medicine, Berlin 13125, Germany; Institute of Pharmacology and Toxicology and Rudolf Virchow Center, University of Würzburg, Würzburg 97070, Germany

Laura J. Humphrys – Institute of Pharmacy, University of Regensburg, Regensburg 93053, Germany

Martin Nagl – Institute of Pharmacy, University of Regensburg, Regensburg 93053, Germany

Ulla Seibel – Institute of Pharmacy, University of Regensburg, Regensburg 93053, Germany

Martin J. Lohse – Max Delbrück Center for Molecular Medicine, Berlin 13125, Germany; Institute of Pharmacology and Toxicology and Rudolf Virchow Center, University of Würzburg, Würzburg 97070, Germany; ISAR Bioscience Institute, Planegg 82152, Germany

Complete contact information is available at:

<https://pubs.acs.org/doi/10.1021/acs.jmedchem.1c01089>

Author Contributions

N.R. contributed to the following: chemistry, structural analysis, FACS experiments, fluorescence properties, radioligand binding studies, and manuscript writing. L.G. contributed to the following: conception, project administration, NanoBRET studies, and manuscript writing. H.S. contributed to the following: the G₁₂-BRET sensor and studies and manuscript writing. J.M. contributed to the following: TIRF microscopy and manuscript writing. A.I. contributed to the following: confocal microscopy and manuscript writing. L.J.H. contributed to the following: off-target screening, live cell ELISA, and manuscript writing. M.N. contributed to the following: chemistry, radioligand binding studies, and manuscript writing. U.S. contributed to the following: cell culture and manuscript writing. M.J.L. contributed to the following: providing infrastructure and manuscript writing. S.P. con-

tributed to the following: conception, project administration, FACS experiments, and manuscript writing. The manuscript was written through contributions of all authors. All authors have given approval to the final version of the manuscript.

Funding

This work was supported by the Deutsche Forschungsgemeinschaft (DFG, German Research Foundation – 427840891) to H.S. Financial support by the Deutsche Forschungsgemeinschaft (DFG, Research Training Group GRK1910) is gratefully acknowledged (L.G., L.J.H.). Financial support by the graduate school “Receptor Dynamics” of the Elite Network of Bavaria (ENB) is gratefully acknowledged (N.R., H.S., J.M., A.I., M.N., S.P.). Financial support by the EU training network Oncor-net and the SFB 1423 is gratefully acknowledged (A.I., M.J.L.).

Notes

The authors declare no competing financial interest. Ligand and plasmids are available from the corresponding authors upon reasonable request.

ACKNOWLEDGMENTS

We thank Prof. Dr. Sigurd Elz and Prof. Dr. Gunnar Schulte for providing infrastructure and Dr. Ulrike Zabel for support in cloning the NLuc tagged β_1 adrenoceptor. We thank Denise Mönnich for support in cloning the NLuc tagged D₁ receptor. We thank Prof. Dr. Gunnar Schulte (mouse smoothed receptor) and Prof. Dr. Stephen J. Hill (adenosine A₃ receptor) for providing the respective NLuc receptor constructs.

ABBREVIATIONS

aq, aqueous; a.u., arbitrary units; AU, absorption units; Bq, becquerel; B_{max} , total number of receptors in a sample; br, broad; BRET, bioluminescence resonance energy transfer; BSA, bovine serum albumin; CDCl₃, deuterated chloroform; CHO, Chinese hamster ovary cells; CI, confidence interval; clob, clobenpropit; cpm, counts per minute; CRC, concentration response curve; Cy3, cyanine dye 3; DAD, diode array detector; dd, doublet of doublets; DIPEA, diisopropylethylamine; DMEM, Dulbecco's modified Eagle medium; DMSO- d_6 , deuterated DMSO; dt, doublet of triplets; EDC-HCl, 1-ethyl-3-(3-dimethylaminopropyl)carbodiimide hydrochloride; eq, equivalent; EtOAc, ethyl acetate; EtOH, ethanol; FCS, fetal bovine serum; G418, geneticin; $G\alpha_{12}$, α -subunit of the G_{12} protein that mediates inhibition of adenylyl cyclase; $G\beta_1\gamma_2$, G protein β_1 - and γ_2 -subunit; HBSS, Hank's balanced salt solution; HOBt, 1-hydroxybenzotriazole; H₂O, water; HEK293, human embryonic kidney 293 cells; HEK293T, human embryonic kidney 293 T cells; HEPES, 2-[4-(2-hydroxyethyl)piperazin-1-yl]ethanesulfonic acid; His, histamine; H_xR_s, histamine receptor subtype x; imet, imetit; k , retention (or capacity) factor (HPLC); K_b , dissociation constant obtained from functional assays; K_d , dissociation constant obtained from a saturation binding experiment; K_i , dissociation constant obtained from a competition binding experiment; k_{in} , kinetic; k_{obs} , observed association rate constant; k_{off} , dissociation rate constant; k_{on} , association rate constant; MeCN, acetonitrile; CD₃OD, deuterated methanol; MeOH, methanol; MW, microwave; N, normality; NanoBRET, NanoLuc luciferase-based bioluminescence resonance energy transfer; NEt₃, triethylamine; NLuc, NanoLuc fragment; PE, petroleum ether; pEC_{50} , negative logarithm of the half-maximum activity concentration in M; pH, potential or power of hydrogen; pito, pitolisant; pK_b , negative logarithm of

K_b in M; pK_i , negative logarithm of K_i in M; ppm, parts per million; PTFE, polytetrafluoroethylene; RAMH, (R)-(-)- α -methylhistamine; RP-HPLC, reversed-phase HPLC; Q-TOF, quadrupole time of flight; RET, resonance energy transfer; sat, saturation; SAMH, (S)-(+)- α -methylhistamine; SD, standard deviation; s, second; SEM, standard error of the mean; t_0 , dead time; 5-TAMRA NHS-ester, 5-carboxytetramethylrhodamine succinimidyl ester; thio, thioperamide; TIRF, total internal reflection fluorescence; t_R , retention time; TR-FRET, time-resolved Förster resonance energy transfer; τ_{ass} , association time constant; τ_{diss} , dissociation time constant; WLL, white light laser; Z-cmpd, Z27743747

REFERENCES

- (1) Arrang, J.-M.; Garbarg, M.; Schwartz, J.-C. Auto-Inhibition of Brain Histamine Release Mediated by a Novel Class (H₃) of Histamine Receptor. *Nature* **1983**, *302*, 832–837.
- (2) Clark, E. A.; Hill, S. J. Sensitivity of Histamine H₃ Receptor Agonist-Stimulated [³⁵S] GTP γ [S] Binding to Pertussis Toxin. *Eur. J. Pharmacol.* **1996**, *296*, 223–225.
- (3) Takeshita, Y.; Watanabe, T.; Sakata, T.; Munakata, M.; Ishibashi, H.; Akaike, N. Histamine Modulates High-Voltage-Activated Calcium Channels in Neurons Dissociated from the Rat Tubero-mammillary Nucleus. *Neuroscience* **1998**, *87*, 797–805.
- (4) Arrang, J.-M.; Devaux, B.; Chodkiewicz, J.-P.; Schwartz, J.-C. H₃-Receptors Control Histamine Release in Human Brain. *J. Neurochem.* **1988**, *51*, 105–108.
- (5) Lovenberg, T. W.; Roland, B. L.; Wilson, S. J.; Jiang, X.; Pyati, J.; Huvar, A.; Jackson, M. R.; Erlander, M. G. Cloning and Functional Expression of the Human Histamine H₃ Receptor. *Mol. Pharmacol.* **1999**, *55*, 1101–1107.
- (6) Rapanelli, M. The Magnificent Two: Histamine and the H₃ Receptor as Key Modulators of Striatal Circuitry. *Prog. Neuro-Psychopharmacol. Biol. Psychiatry* **2017**, *73*, 36–40.
- (7) Ferrada, C.; Ferré, S.; Casadó, V.; Cortés, A.; Justinova, Z.; Barnes, C.; Canela, E. I.; Goldberg, S. R.; Leurs, R.; Lluís, C.; Franco, R. Interactions between Histamine H₃ and Dopamine D₂ Receptors and the Implications for Striatal Function. *Neuropharmacology* **2008**, *55*, 190–197.
- (8) Goodchild, R. E.; Court, J. A.; Hobson, I.; Piggott, M. A.; Perry, R. H.; Ince, P.; Jaros, E.; Perry, E. K. Distribution of Histamine H₃ -Receptor Binding in the Normal Human Basal Ganglia: Comparison with Huntington's and Parkinson's Disease Cases: Histamine H₃-Receptors in the Human Basal Ganglia. *Eur. J. Neurosci.* **1999**, *11*, 449–456.
- (9) Moreno-Delgado, D.; Puigdemívol, M.; Moreno, E.; Rodríguez-Ruiz, M.; Botta, J.; Gasperini, P.; Chiarlone, A.; Howell, L. A.; Scarselli, M.; Casadó, V.; Cortés, A.; Ferré, S.; Guzmán, M.; Lluís, C.; Alberch, J.; Canela, E. I.; Ginés, S.; McCormick, P. J. Modulation of Dopamine D₁ Receptors via Histamine H₃ Receptors Is a Novel Therapeutic Target for Huntington's Disease. *eLife* **2020**, *9*, No. e51093.
- (10) Rodríguez-Ruiz, M.; Moreno, E.; Moreno-Delgado, D.; Navarro, G.; Mallol, J.; Cortés, A.; Lluís, C.; Canela, E. I.; Casadó, V.; McCormick, P. J.; Franco, R. Heteroreceptor Complexes Formed by Dopamine D₁, Histamine H₃, and N-Methyl-D-Aspartate Glutamate Receptors as Targets to Prevent Neuronal Death in Alzheimer's Disease. *Mol. Neurobiol.* **2017**, *54*, 4537–4550.
- (11) Rapanelli, M.; Frick, L.; Pogorelov, V.; Ohtsu, H.; Bitó, H.; Pittenger, C. Histamine H₃R Receptor Activation in the Dorsal Striatum Triggers Stereotypies in a Mouse Model of Tic Disorders. *Transl. Psychiatry* **2017**, *7*, e1013–e1013.
- (12) Syed, Y. Y. Pitolisant: First Global Approval. *Drugs* **2016**, *76*, 1313–1318.
- (13) Pullen, L. C.; Picone, M.; Tan, L.; Johnston, C.; Stark, H. Cognitive Improvements in Children with Prader-Willi Syndrome Following Pitolisant Treatment—Patient Reports. *J. Pediatr. Pharmacol. Ther.* **2019**, *24*, 166–171.

- (14) Emami-Nemini, A.; Roux, T.; Leblay, M.; Bourrier, E.; Lamarque, L.; Trinquet, E.; Lohse, M. J. Time-Resolved Fluorescence Ligand Binding for G Protein-Coupled Receptors. *Nat. Protoc.* **2013**, *8*, 1307–1320.
- (15) Stoddart, L. A.; Johnstone, E. K. M.; Wheal, A. J.; Goulding, J.; Robers, M. B.; Machleidt, T.; Wood, K. V.; Hill, S. J.; Pflieger, K. D. G. Application of BRET to Monitor Ligand Binding to GPCRs. *Nat. Methods* **2015**, *12*, 661–663.
- (16) Stoddart, L. A.; Kilpatrick, L. E.; Hill, S. J. NanoBRET Approaches to Study Ligand Binding to GPCRs and RTKs. *Trends Pharmacol. Sci.* **2018**, *39*, 136–147.
- (17) Axelrod, D. Cell-Substrate Contacts Illuminated by Total Internal Reflection Fluorescence. *J. Cell Biol.* **1981**, *89*, 141–145.
- (18) Sako, Y.; Minoghchi, S.; Yanagida, T. Single-Molecule Imaging of EGFR Signalling on the Surface of Living Cells. *Nat. Cell Biol.* **2000**, *2*, 168–172.
- (19) Kuder, K.; Kiec-Kononowicz, K. Fluorescent GPCR Ligands as New Tools in Pharmacology. *Curr. Med. Chem.* **2008**, *15*, 2132–2143.
- (20) Kuder, K. J.; Kottke, T.; Stark, H.; Ligneau, X.; Camelin, J.-C.; Seifert, R.; Kiec-Kononowicz, K. Search for Novel, High Affinity Histamine H₃ Receptor Ligands with Fluorescent Properties. *Inflammation Res.* **2010**, *59*, 247–248.
- (21) Tomasch, M.; Schwed, J. S.; Paulke, A.; Stark, H. Bodilisant—A Novel Fluorescent, Highly Affine Histamine H₃ Receptor Ligand. *ACS Med. Chem. Lett.* **2013**, *4*, 269–273.
- (22) Kuder, K.; Kiec-Kononowicz, K. Fluorescent GPCR Ligands as New Tools in Pharmacology-Update, Years 2008- Early 2014. *Curr. Med. Chem.* **2014**, *21*, 3962–3975.
- (23) Bartole, E.; Grätz, L.; Littmann, T.; Wifling, D.; Seibel, U.; Buschauer, A.; Bernhardt, G. UR-DEBa242: A Py-5-Labeled Fluorescent Multipurpose Probe for Investigations on the Histamine H₃ and H₄ Receptors. *J. Med. Chem.* **2020**, 5297.
- (24) Drakopoulos, A.; Decker, M. Development and Biological Applications of Fluorescent Opioid Ligands. *ChemPlusChem* **2020**, *85*, 1354–1364.
- (25) Apodaca, R.; Dvorak, C. A.; Xiao, W.; Barbier, A. J.; Boggs, J. D.; Wilson, S. J.; Lovenberg, T. W.; Carruthers, N. I. A New Class of Diamine-Based Human Histamine H₃ Receptor Antagonists: 4-(Aminoalkoxy)Benzylamines. *J. Med. Chem.* **2003**, *46*, 3938–3944.
- (26) Wingen, K.; Schwed, J. S.; Isensee, K.; Weizel, L.; Živković, A.; Odazic, D.; Stark, H. Benzylpiperidine Variations on Histamine H₃ Receptor Ligands for Improved Drug-Likeness. *Bioorg. Med. Chem. Lett.* **2014**, *24*, 2236–2239.
- (27) Kshirsagar, T.; Nakano, A. H.; Law, P.-Y.; Elde, R.; Portoghese, P. S. NT14F: A Non-Peptide Fluorescent Probe Selective for Functional Delta Opioid Receptors. *Neurosci. Lett.* **1998**, *249*, 83–86.
- (28) Grätz, L.; Tropmann, K.; Bresinsky, M.; Müller, C.; Bernhardt, G.; Pockes, S. NanoBRET Binding Assay for Histamine H₂ Receptor Ligands Using Live Recombinant HEK293T Cells. *Sci. Rep.* **2020**, *10*, 13288.
- (29) Rüttinger, S.; Lamarre, B.; Knight, A. E. Single Molecule Genotyping by TIRF Microscopy. *J. Fluoresc.* **2008**, *18*, 1021–1026.
- (30) Laasfeld, T.; Ehrminger, R.; Tahk, M.-J.; Veiksina, S.; Kölvart, K. R.; Min, M.; Kopanchuk, S.; Rinken, A. Budded Baculoviruses as a Receptor Display System to Quantify Ligand Binding with TIRF Microscopy. *Nanoscale* **2021**, *13*, 2436–2447.
- (31) Qiu, B.; Simon, M. C. BODIPY 493/503 Staining of Neutral Lipid Droplets for Microscopy and Quantification by Flow Cytometry. *Bio-Protoc.* **2016**, *6*, No. e1912.
- (32) Newman, M. S.; Barbee, T. G.; Blakesley, C. N.; Zia-ud-Din; Gromelski, S., Jr.; Khanna, V. K.; Lee, L.-F.; Radhakrishnan, J.; Robey, R. L. High-Dilution Cyclization of Polyoxapentacosanodinitriles. *J. Org. Chem.* **1975**, *40*, 2863–2870.
- (33) Lahav, D.; Liu, B.; van den Berg, R. J. B. H. N.; van den Nieuwendijk, A. M. C. H.; Wennekes, T.; Ghisaidoobe, A. T.; Breen, I.; Ferraz, M. J.; Kuo, C.-L.; Wu, L.; Geurink, P. P.; Ova, H.; van der Marel, G. A.; van der Stelt, M.; Boot, R. G.; Davies, G. J.; Aerts, J. M. F. G.; Overkleeft, H. S. A Fluorescence Polarization Activity-Based Protein Profiling Assay in the Discovery of Potent, Selective Inhibitors for Human Nonlysosomal Glucosylceramidase. *J. Am. Chem. Soc.* **2017**, *139*, 14192–14197.
- (34) Iyer, S. S.; Anderson, A. S.; Reed, S.; Swanson, B.; Schmidt, J. G. Synthesis of Orthogonal End Functionalized Oligoethylene Glycols of Defined Lengths. *Tetrahedron Lett.* **2004**, *45*, 4285–4288.
- (35) Baumeister, P.; Erdmann, D.; Biselli, S.; Kagermeier, N.; Elz, S.; Bernhardt, G.; Buschauer, A. [³H]UR-DE257: Development of a Tritium-Labeled Squaramide-Type Selective Histamine H₂ Receptor Antagonist. *ChemMedChem* **2015**, *10*, 83–93.
- (36) Igel, P.; Schnell, D.; Bernhardt, G.; Seifert, R.; Buschauer, A. Tritium-Labeled N¹-[3-(1 H -Imidazol-4-yl)Propyl]- N²-Propionylguanidine ([³H]UR-PI294), a High-Affinity Histamine H₃ and H₄ Receptor Radioligand. *ChemMedChem* **2009**, *4*, 225–231.
- (37) Schihada, H.; Shekhani, R.; Schulte, G. Quantitative assessment of constitutive G protein-coupled receptor activity with BRET-based G protein biosensors. *bioRxiv* **2021**, DOI: 10.1101/2021.02.05.429900.
- (38) Windaus, A.; Vogt, W. Synthesis of Imidazolylethylamine. *Ber. Dtsch. Chem. Ges.* **1907**, *40*, 3685–3691.
- (39) Garbarg, M.; Arrang, J. M.; Rouleau, A.; Ligneau, X.; Tuong, M. D.; Schwartz, J. C.; Ganellin, C. S-[2-(4-Imidazolyl) Ethyl] Isothiourea, a Highly Specific and Potent Histamine H₃ Receptor Agonist. *J. Pharmacol. Exp. Ther.* **1992**, *263*, 304–310.
- (40) Arrang, J.-M.; Garbarg, M.; Lancelo, J.-C.; Lecomte, J.-M.; Pollard, H.; Robba, M.; Schunack, W.; Schwartz, J.-C. Highly Potent and Selective Ligands for Histamine H₃-Receptors. *Nature* **1987**, *327*, 117–123.
- (41) Van der Goot, H.; Schepers, M. J. P.; Sterk, G. J.; Timmerman, H. Isothiourea Analogues of Histamine as Potent Agonists or Antagonists of the Histamine H₃-Receptor. *Eur. J. Med. Chem.* **1992**, *27*, 511–517.
- (42) Schaller, D.; Hagenow, S.; Stark, H.; Wolber, G. Ligand-Guided Homology Modeling Drives Identification of Novel Histamine H₃ Receptor Ligands. *PLoS One* **2019**, *14*, No. e0218820.
- (43) Ligneau, X.; Perrin, D.; Landais, L.; Camelin, J.-C.; Calmels, T.; Berrebi-Bertrand, I.; Lecomte, J.-M.; Parmentier, R.; Anacleit, C.; Lin, J.-S.; Bertaina-Anglade, V.; la Rochelle, C. D.; d’Aniello, F.; Rouleau, A.; Gbahou, F.; Arrang, J. M.; Ganellin, C. R.; Stark, H.; Schunack, W.; Schwartz, J.-C. BF2.649 [1-{3-[3-(4-Chlorophenyl) propoxy]-propyl}piperidine, Hydrochloride], a Nonimidazole Inverse Agonist/Antagonist at the Human Histamine H₃ Receptor: Preclinical Pharmacology. *J. Pharmacol. Exp. Ther.* **2007**, *320*, 365–375.
- (44) Wulff, B. S.; Hastrup, S.; Rimvall, K. Characteristics of Recombinantly Expressed Rat and Human Histamine H₃ Receptors. *Eur. J. Pharmacol.* **2002**, *453*, 33–41.
- (45) Lim, H. D.; van Rijn, R. M.; Ling, P.; Bakker, R. A.; Thurmond, R. L.; Leurs, R. Evaluation of Histamine H₁-, H₂-, and H₃-Receptor Ligands at the Human Histamine H₄ Receptor: Identification of 4-Methylhistamine as the First Potent and Selective H₄ Receptor Agonist. *J. Pharmacol. Exp. Ther.* **2005**, *314*, 1310–1321.
- (46) Schihada, H.; Ma, X.; Zabel, U.; Vischer, H. F.; Schulte, G.; Leurs, R.; Pockes, S.; Lohse, M. J. Development of a Conformational Histamine H₃ Receptor Biosensor for the Synchronous Screening of Agonists and Inverse Agonists. *ACS Sens.* **2020**, *5*, 1734–1742.
- (47) Mocking, T. A. M.; Verweij, E. W. E.; Vischer, H. F.; Leurs, R. Homogeneous, Real-Time NanoBRET Binding Assays for the Histamine H₃ and H₄ Receptors on Living Cells. *Mol. Pharmacol.* **2018**, *94*, 1371–1381.
- (48) Pockes, S.; Wifling, D.; Keller, M.; Buschauer, A.; Elz, S. Highly Potent, Stable, and Selective Dimeric Hetarylpropylguanidine-Type Histamine H₂ Receptor Agonists. *ACS Omega* **2018**, *3*, 2865–2882.
- (49) Gentzsch, C.; Seier, K.; Drakopoulos, A.; Jobin, M.-L.; Lanoiselée, Y.; Koszegi, Z.; Maurel, D.; Soumier, R.; Hübner, H.; Gmeiner, P.; Granier, S.; Calebiro, D.; Decker, M. Selective and Wash-Resistant Fluorescent Dihydrocodeinone Derivatives Allow Single-Molecule Imaging of M-Opioid Receptor Dimerization. *Am. Ethnol.* **2020**, *132*, 6014–6020.
- (50) Sungkaworn, T.; Jobin, M.-L.; Burnecki, K.; Weron, A.; Lohse, M. J.; Calebiro, D. Single-Molecule Imaging Reveals Receptor-G

Protein Interactions at Cell Surface Hot Spots. *Nature* **2017**, *550*, 543–547.

(51) Möller, J.; Isbilir, A.; Sungkaworn, T.; Osberg, B.; Karathanasis, C.; Sunkara, V.; Grushevskiy, E. O.; Bock, A.; Annibale, P.; Heilemann, M.; Schütte, C.; Lohse, M. J. Single-Molecule Analysis Reveals Agonist-Specific Dimer Formation of μ -Opioid Receptors. *Nat. Chem. Biol.* **2020**, *16*, 946–954.

(52) Soave, M.; Stoddart, L. A.; Brown, A.; Woolard, J.; Hill, S. J. Use of a New Proximity Assay (NanoBRET) to Investigate the Ligand-Binding Characteristics of Three Fluorescent Ligands to the Human β_1 -Adrenoceptor Expressed in HEK-293 Cells. *Pharmacol. Res. Perspect.* **2016**, *4*, No. e00250.

(53) Kozielwicz, P.; Bowin, C.-F.; Turku, A.; Schulte, G. A NanoBRET-Based Binding Assay for Smoothed Allows Real-Time Analysis of Ligand Binding and Distinction of Two Binding Sites for BODIPY-Cyclopamine. *Mol. Pharmacol.* **2020**, *97*, 23–34.

(54) Grätz, L.; Laasfeld, T.; Allikalt, A.; Gruber, C. G.; Pegoli, A.; Tahk, M.-J.; Tsernant, M.-L.; Keller, M.; Rinke, A. BRET-and Fluorescence Anisotropy-Based Assays for Real-Time Monitoring of Ligand Binding to M_2 Muscarinic Acetylcholine Receptors. *Biochim. Biophys. Acta Mol. Cell Res.* **2021**, *1868*, 118930.

(55) Allikalt, A.; Purkayastha, N.; Flad, K.; Schmidt, M. F.; Tabor, A.; Gmeiner, P.; Hübner, H.; Weikert, D. Fluorescent Ligands for Dopamine D_2/D_3 Receptors. *Sci. Rep.* **2020**, *10*, 21842.

(56) Pándy-Szekeres, G.; Munk, C.; Tsonkov, T. M.; Mordalski, S.; Harpsøe, K.; Hauser, A. S.; Bojarski, A. J.; Gloriam, D. E. GPCRdb in 2018: Adding GPCR Structure Models and Ligands. *Nucleic Acids Res.* **2018**, *46*, D440–D446.

(57) Staszewski, M.; Nelic, D.; Jończyk, J.; Dubiel, M.; Frank, A.; Stark, H.; Bajda, M.; Jakubik, J.; Walczyński, K. Guanidine Derivatives: How Simple Structural Modification of Histamine H_3R Antagonists Has Led to the Discovery of Potent Muscarinic M_2R/M_4R Antagonists. *ACS Chem. Neurosci.* **2021**, *12*, 2503–2519.

(58) Perepichka, I. F.; Besbes, M.; Levillain, E.; Sallé, M.; Roncali, J. Hydrophilic Oligo(Oxyethylene)-Derivatized Poly(3,4-Ethylenedioxythiophenes): Cation-Responsive Optoelectrochemical Properties and Solid-State Chromism. *Chem. Mater.* **2002**, *14*, 449–457.

(59) Goswami, L. N.; Houston, Z. H.; Sarma, S. J.; Jalisatgi, S. S.; Hawthorne, M. F. Efficient Synthesis of Diverse Heterobifunctionalized Clickable Oligo (Ethylene Glycol) Linkers: Potential Applications in Bioconjugation and Targeted Drug Delivery. *Org. Biomol. Chem.* **2013**, *11*, 1116–1126.

(60) Baell, J. B.; Holloway, G. A. New Substructure Filters for Removal of Pan Assay Interference Compounds (PAINS) from Screening Libraries and for Their Exclusion in Bioassays. *J. Med. Chem.* **2010**, *53*, 2719–2740.

(61) Aldrich, C.; Bertozzi, C.; Georg, G. I.; Kiessling, L.; Lindsley, C.; Liotta, D.; Merz, K. M.; Schepartz, A.; Wang, S. The Ecstasy and Agony of Assay Interference Compounds. *ACS Cent. Sci.* **2017**, *3*, 143–147.

(62) Keller, M.; Erdmann, D.; Pop, N.; Pluym, N.; Teng, S.; Bernhardt, G.; Buschauer, A. Red-Fluorescent Argininamide-Type NPY Y_1 Receptor Antagonists as Pharmacological Tools. *Bioorg. Med. Chem.* **2011**, *19*, 2859–2878.

(63) Cheng, Y.-C.; Prusoff, W. H. Relationship between the Inhibition Constant (K_i) and the Concentration of the Inhibitor Which Causes 50 per Cent Inhibition (I_{50}) of an Enzymatic Reaction. *Biochem. Pharmacol.* **1973**, *22*, 3099–3108.

(64) Schindelin, J.; Arganda-Carreras, I.; Frise, E.; Kaynig, V.; Longair, M.; Pietzsch, T.; Preibisch, S.; Rueden, C.; Saalfeld, S.; Schmid, B.; Tinevez, J.-Y.; White, D. J.; Hartenstein, V.; Eliceiri, K.; Tomancak, P.; Cardona, A. Fiji: An Open-Source Platform for Biological-Image Analysis. *Nat. Methods* **2012**, *9*, 676–682.

(65) Jaqaman, K.; Loerke, D.; Mettlen, M.; Kuwata, H.; Grinstein, S.; Schmid, S. L.; Danuser, G. Robust Single-Particle Tracking in Live-Cell Time-Lapse Sequences. *Nat. Methods* **2008**, *5*, 695–702.

(66) İsbilir, A.; Möller, J.; Arimont, M.; Bobkov, V.; Perpiñá-Viciano, C.; Hoffmann, C.; Inoue, A.; Heukers, R.; de Graaf, C.; Smit, M. J.; Annibale, P.; Lohse, M. J. Advanced fluorescence microscopy reveals

disruption of dynamic CXCR4 dimerization by subpocket-specific inverse agonists. *Proc. Natl. Acad. Sci. U.S.A.* **2020**, *117*, 29144–29154.